Norwegian University
of Life Sciences

Whispering Gallery Resonances in Dielectric Disk

Frida Helen Maria Torgersen
Environmental Physics and Renewable Energy

Dedication

This thesis is dedicated to the bright memory of

Peter Holum Normann

(20.12.1988-13.03.2016)

May the sun always shine for you.

Preface

This thesis is the fulfilment of my Master of Science at the Norweigan University of Life Science (NMBU).

The interesting subject of this thesis gave me the opportunity to write about energy physics and solar energy. Solar energy is one of my passions and was shared with Peter Holum Normann, to whom this thesis is dedicated. Peter's vision was to cover all roofs in the world with solar cells. Mabey the project this thesis is written for, will in future contribute that more people can afford solar cells and install them on their roofs. A special thank to my supervisor Prof. Achim Kohler for giving me the opportunity to write about this subject. I want to thank Achim for all help, guidance and his contagious engagement. The help from talented Dr. Rozalia Lukacs made it possible for me to fulfil a thesis with the results presented. I want to thank Rozalia for the help with the Matlab programs and all good advice. I also want to thank Maren Anna Branstad for discussions, friendship and help.

My husband Jørgen and my children Isak and Oliver fills my life with love. I want to thank them for their patience and support. I also want to thank my parents, for their guidance and love and my siblings Fredrik, Daniel and Emelie for inspiration and friendship.

Ås, May 13, 2016

Frida Helen Maria Torgersen

IV

Abstract

Dielectric nanostructures, such as spherical nanoimprints, have emerged as a promising alternative for efficiency enhancement by light-trapping in thin solar cells. Some of the effectivity increase can be explained by resonant modes called Whispering gallery modes. The rationale of this increase is not fully understood and the hypothesis is that nanostructure parameters and coupled modes can be directly related to the absorption resonance. In order to study Whispering gallery modes and coupled modes in nanostructures in addition to the parameters of the nanostructures, a numerical algorithm was developed. The numerical algorithm was based on the Lippmann-Schwinger equation for the scattering of a two-dimensional plane wave at multiple coupled disk arrays. The aim of this thesis was to verify the numerical algorithm using two analytical solutions, namely the scattering of a plane wave at a single disk and the scattering of a spherical wave at a single disk. All three solutions were solved for a simple and comparable problem, i.e. scattering at a single disk. The comparison between the analytical plane wave scattering solution and the numerical solution based on the Lippmann-Schwinger equation showed agreement. The appearance and type of resonance found in the numerical solution was highly dependent on the grid ressolution. Based on results of this thesis it is obvious that the numerical solution based on the Lippmann-Schwinger equation is a stable program converging to the exact result, when the grid resolution is increased. We further expected to find the resonance wavenumbers that were detected in the analytical plane wave scattering program, by considering the S-matrix of the analytical spherical wave scattering. However, a comparison between these solutions revealed no similarities. In order to study the analytical solution for the spherical wave in this thesis we considered only the real part of the S-matrix. An analysis of the real and imaginary part of the S-matrix seems to be required to study the resonances in the analytical spherical wave scattering.

Sammendrag

Nanostrukturer med dielektriske egenskaper, slik som sfæriske nanoavtrykk, har vist seg som et lovende alternativ for effektivisering av lys-fangst i tynne solceller. Noe av den økte effektiviteten kan forklares med resonanser kalt Whispering gallery moder. Begrunnelsen for denne økningen er ikke fullt forstått, og hypotesen er at nanostrukturens parametere og koblede moder kan være direkte relatert til absorpsjon. En numerisk algoritme basert på Lippmann-Schwinger ligningen for spredning av en to-dimensjonal planbølge på flere koblede disksett, ble utviklet for å studere Whispering gallery moder og koblede moder i nanostrukturer samt parameterne av nanostrukturene. Målet for denne oppgaven var å verifisere den numeriske algoritmen ved hjelp av to analytiske løsninger, nemlig spredningen av en planbølge på en enkel disk og spredningen av en sfærisk bølge på en enkel disk. Alle tre program ble løst for et enkelt og sammenlignbart problem, dvs. spredning ved en enkelt disk. En sammenligning mellom den analytiske planbølge løsningen og den numeriske løsningen basert på Lippmann-Schwinger ligningen viste Whispering gallery resonanser på omtrent samme bølgenummer. Plasseringen av bølgenummer og type resonans som oppstår med den numeriske løsningen er sterkt avhengig av gitter oppløsningen. Basert på resultatene i denne oppgaven er det åpenbart at den numeriske løsningen basert på Lippmann-Schwinger ligningen er et stabil program som konvergerer til det nøyaktige resultatet, når gitteret oppløsningen økes. Det var også ventet noen likheter mellom den analytiske planbølgeløsningen og den analytiske sfæriske bølgeløsningen. En sammenligning mellom disse løsningene viste ingen likheter. For å studere den analytiske løsningen for den sfæriske bølgen i denne avhandling er det bare sett på den reelle delen av S-matrisen. En analyse av den reelle og imaginære delen av S-matrisen er nødvendig for å studere resonanser i den analytiske sfæriske bølgeløsningen.

Table of content

1 Introduction

Warming of the climate system is unequivocal, and since the 1950s, many of the observed changes are unprecedented over decades to millennia. The atmosphere and ocean have warmed, the amounts of snow and ice have diminished, and sea level has risen.   (Pachauri et al. 2014)

The expanding global population and subsequent increasing demand for energy is aggravating the challenges related to climate change. According to the IPCC's Fifth Assessment Report, burning fossil fuel is the primary driving factor in global warming. Thus, fossil fuels need to be replaced by green renewable energy. A very promising green energy is solar energy.

Bells Labs presented in 1954 the first practical silicon solar cells with an efficiency of 5.7%. The cost to produce solar cells was high and therefore primary used in space applications to provide power to satellites (Chen 2011). In recent years, falling costs along with increased efficiency made solar cells one of the most common renewable energy systems. For commercial and private use, the market offers cost-effective solar cells with an efficiency of around 10-20%. The solar cell industry is striving to meet the demand in the market and to come below grid parity. Because raw materials are in short supply, and production costs are high, researchers started to investigate how to reduce materials of solar cells, for example by manufacturing thinner solar cells.

Solar cells convert incoming sunlight into electrical energy. To achieve this, the cells need to absorb light. The thickness, that varies from around 150-300 μm, is usually proportional to light absorption inside the solar cell (Grandidier et al. 2011). Longer optical path length, i.e. the distance an unabsorbed photon travels inside the solar cell, enhances the light absorption. One of the most common methods used to increase the optical path length, is light-trapping in the photovoltaic material. By adding front and rear surface texturing, the probability for internal reflection is increased and light is trapped by multiple passes inside the solar cell. Another more advanced type of light-trapping is effective photon management. Light-trapping (spheres(Eisenlohr et al. 2014), cylinders(Wallentin et al. 2013), domes(Zhu et al. 2009)) are coated at the top of the absorbing layer of the solar cell to improve the efficiency enhancement. The idea is to achieve thinner and cheaper solar cells without reducing their effectiveness.

1

Grandidier et. al.'s experimental study (2013) created a promising platform for the potential of effective photon management. The results showed an efficiency increase from 11 %, using wavelength-scale resonant dielectric nanospheres. This increase can be explained by resonant modes called Whispering gallery modes, described by Mie electrical and magnetic modes. Grandidier et. al. verified the efficiency increase numerically by using a Finite Difference Time Domain (FDTD) technique. However, while the efficiency increase of light-trapping nanostructures has been demonstrated, the rationale behind is not understood. It is not clear, how nanostructure parameters such as refractive indices, sizes and forms of nanostructures are directly related to the absorption resonances and thus to increase in efficiency. It is unclear if WGMs or coupled modes, i.e. resonances in the near-field between the spheres, are mainly responsible for the enhanced absorption.

In order to study WGMs and coupled modes in nanostructures, R. Blümel and A. Kohler developed a numerical algorithm based on the Lippmann-Schwinger equation for the scattering of a two-dimensional plane wave at multiple coupled disk arrays, and implemented it in MATLAB (Brandsrud 2015). With this method, different parameters such as sizes, refractive indices and geometrical arrangements of the disks can be investigated. The aim of this thesis was to verify the numerical scattering algorithm based on the Lippmann Schwinger equation by using analytical solutions of the scattering of a plane wave and a spherical wave at one disk. For this thesis, both analytical solutions were implemented numerically in order to compare absorption efficiency of a single disk and wave functions of a single disk for the analytical solutions and the numerical algorithm based on the Lippmann Schwinger equation.

The numerical plane wave scattering algorithm based on the Lippmann-Schwinger equation is presented in section 3.2 and the results from simulations are presented in section 4.2. In section 3.1, an analytical solution for a plane wave impinging at a disk is given. In section 4.1 results of the numerical simulations are presented. The comparison of the analytical solution for a plane wave scatter solution with the numerical algorithm based on the Lippmann Schwinger algorithm is presented in 4.1. The analytical solutions for a spherical wave scattering at a disk are described in section 3.3. Numerical results are presented in section 4.3. The comparison of the analytical solution for a plane wave scatter solution with the analytical solution for a spherical wave scatter solution is presented in section 4.3.

2

2 Theory

2.1 Spherical waves

When light propagates from a point source into free space, the wave's cross section expands with increasing distance from the source, as seen in figure 2.1. Therefore, further away from the source the intensity of the radiation decreases (Oraevsky 2002). This type of waves are called spherical waves. The waves create a wave front at the surface of maximum amplitude. Far away from the point source, the wave can be considered as a plane wave.
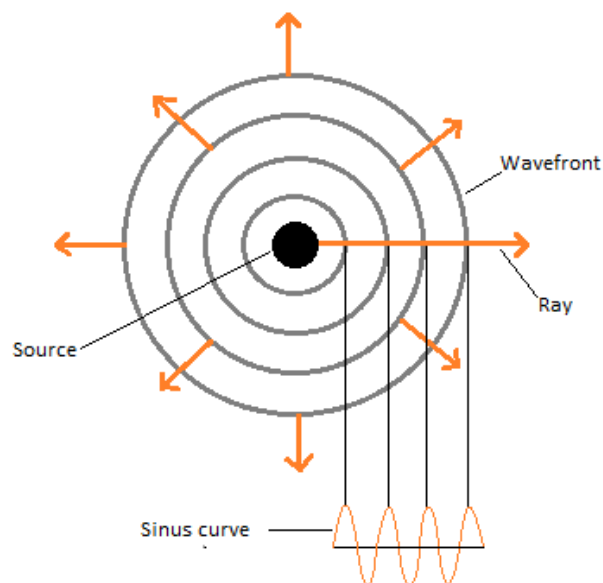

Figure 2.1: Cross section view for spherical waves coming from a point source. One ray can be described with a sinus curve, acting like a plane wave. The waves create a wave front at the surface of maximum amplitude.

Because of spherical symmetry, when a spherical wave impinges a disk, the outgoing scattered wave is also a spherical wave. In this case, the momentum and potential energy are preserved.

2.2 Plane wave

Light is an electromagnetic plane wave that consists of a collection of electric and magnetic fields (Tipler & Mosca 2004; Townsend 2010). The vector product, $\vec{E} \times \vec{B}$, of the electric and magnetic field points into the direction in which the EM-wave propagates with a constant speed, i.e. the speed of light. For a plane wave, propagating in an arbitrary direction, the wave function is given as

$$\vec{A}(x,t) = \vec{A}_0 \cos(\vec{k} \cdot \vec{r} - wt) \tag{2.1}$$

where $\vec{A}_0$ is the amplitude, $\vec{k}$ is the wave vector, which is the angular wavenumber with a direction and magnitude, therefore $|\vec{k}| = k$. The positions vector $\vec{r}$ gives the propagation direction in a two-dimensional space. The time t is a given point in time and ω is the angular wave frequency.
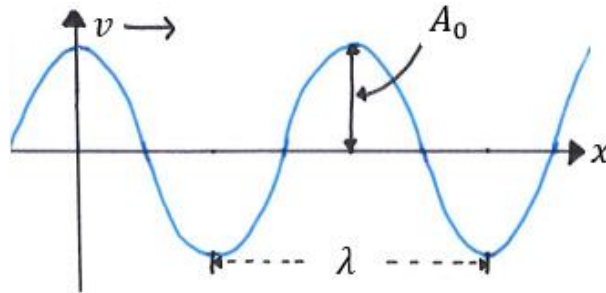

Figure 2.2: Plane wave propagating in x-direction with speed v. A_0 is the amplitude and λ is the wavelength.

In figure 2.2 a wave moves up and down along the x-axis with a repeated pattern every period T. After one period T the wave has moved one wavelength λ. The speed of light c is given by

$$c = \frac{\lambda}{T} = f\lambda \tag{2.2}$$

where the frequency is related to the period via $f = \frac{1}{T}$. The angular wavenumber k is connected to the wavelength λ by

$$k = \frac{2\pi}{\lambda} \tag{2.3}$$

Notice that k has the unit rad/m. The wavenumber ν can be calculated by the relationship

$$\nu = \frac{k}{2\pi} = \frac{1}{\lambda} \tag{2.4}$$

where ν has the unit m^{-1}.

As only two-dimensional problems are treated in this thesis, the algorithms are only solved for two-dimensional space (*x*- and *y*-direction) therefore it is only interesting to look at the electric field. For convenience, $\vec{A}(\vec{r},t)$ can be written as a complex function

$$\vec{E}(\vec{r},t) = \vec{E}_0 e^{i(\vec{k}\cdot\vec{r}-\omega t)} = \vec{A}_0\,cos(\vec{k}\cdot\vec{r}-\omega t) + i\vec{A}_0 sin(\vec{k}\cdot\vec{r}-\omega t) \tag{2.5}$$

Any physical quantity described by $\vec{A}$, is then given by the real part of $\vec{E}(\vec{r},t)$. The wave function can be separated into a product of two functions, $\vec{E}(\vec{r})$ and $T(t)$, dependent on $\vec{r}$ and t, respectively.

$$\vec{\mathrm{E}}(\vec{r},t) = \vec{E}(r)T(t) \tag{2.6}$$

where

$$T(t) = e^{-i\omega t} \tag{2.7}$$

and

$$\vec{E}(\vec{r}) = \vec{E}_0 e^{i\vec{k}\vec{r}} \tag{2.8}$$

Equation (2.8) represent a time independent plane wave, with amplitude $\vec{E}_0$.

2.3 Maxwell wave equation to Helmholtz equation

According to Maxwell's equation, the electric field satisfies the wave equation, which is a second-order partial differential equation (PDE) that describes the propagation of electromagnetic scalar wave in space given by

$$\left(\nabla^2 - \frac{1}{c^2}\frac{\partial^2}{\partial t^2}\right)\vec{E}(\vec{r},t) = 0 \tag{2.9}$$

where c is the speed of light, ∇^2 is the Laplacian operator and $\vec{E}(\vec{r},t)$ is the wave function. When light propagates in a transparent medium with a refractive index n, the speed of light in the medium becomes c/n. The Maxwell wave equation then becomes

$$\left(\nabla^2 - \frac{n^2}{c^2}\frac{\partial^2}{\partial t^2}\right)\tilde{E}(\vec{r},t) = 0 \tag{2.10}$$

Further, we use the ansatz of separated variables $\tilde{E}(\vec{r},t) = \tilde{E}(\vec{r})T(t)$ of the wave function into the wave equation (2.10) and after some simplification this equation can be rewritten

$$\frac{\nabla^2\tilde{E}(\vec{r})}{n^2\tilde{E}(\vec{r})} = \frac{1}{c^2T(t)}\frac{d^2T(t)}{dt^2} \tag{2.11}$$

where the left side is dependent of $\vec{r}$ alone and the right side of t alone. We can set the two sides equal to the same constant, $-k^2$, called the separation constant and obtain two wave equations, one solely for the $\vec{r}$ dependent wave function $\vec{E}(\vec{r})$ and the other solely for the time dependent part of the wave function $T(t)$, given as

$$\frac{\nabla^2\tilde{E}(\vec{r})}{n^2\tilde{E}(\vec{r})} = -k^2 \tag{2.12}$$

and

$$\frac{1}{c^2\tilde{T}(t)}\frac{d^2\tilde{T}(t)}{dt^2} = -k^2 \tag{2.13}$$

where k now is the angular wavenumber, ∇^2 is the Laplacian operator.

From equation (2.12) we obtain the Helmholtz equation

$$(\nabla^2 + \kappa^2)\vec{E}(\vec{r}) = 0 \qquad (2.14)$$

that represents the time-independent form of the wave equation, where κ is the angular wavenumber in the medium given as $\kappa = kn$. Note that for a wave propagating in free space, $n = 1$. As an approximation we replace the plane vector wave $\vec{E}(\vec{r})$, by the single component $\Psi(\vec{r})$ and use it as a wave function of a two-dimensional system. We will in the following examine the scalar wave function $\Psi(\vec{r})$ as an approximation for full 3-dimensional electromagnetic theory (Kirsch & Hettlich 2009). The Helmholtz equation becomes

$$(\nabla^2 + \kappa^2)\Psi(\vec{r}) = 0 \qquad (2.15)$$

where $\Psi(\vec{r})$ is the wave function and $\vec{r}$ is the position vector in the *x*- and *y*-plane.

2.4 Whispering gallery modes

In 1878 Lord Rayleigh visited St Paul´s Cathedral in London. Here Rayleigh experienced the phenomena that he later called "whispering-gallery waves"(Oraevsky 2002). At the bottom of the dome in the Cathedral lies an interior gallery, called the whispering gallery. The gallery is a concave cylinder shaped room. If a person whispers on one side of the room, another person can hear the whisper loud and clear on the other side of the room, 34 m away. Because of the concave surface of the gallery, the wave travels along the surface of the walls. As a result, the sound intensity remains high. This is explained by the fact that the wave cross-section expands much slower than it would in free space. The physical explanation of the phenomena was given analytically by Rayleigh. Later it was discovered that electromagnetic waves inside dielectric and highly symmetric structures also exhibit "Whispering galley modes".

When light is scattered by a homogenous and highly symmetric structure, e.g. a sphere, resonances in the interior of the sphere may be generated, which appear at distinct wavelengths. For simplicity, we consider scattering of an electromagnetic wave in two dimensions, i.e. at a disk. These resonances typically appear when the size of the disk, is approximately at the same scale as the wavelength of the electromagnetic radiation. The exact wavelength that exhibits the resonance and the type of the resonance, depends on the refractive index ratio between the disk and the surrounding medium and the geometry/size of the disk. Whispering gallery modes (WGM) are resonances, that appear when light is trapped inside the disk and the disk is lightening brightly. In whispering gallery mode resonances, the

trapped wave travels around the inside of the disk. Bright nodes arranged in a regular order inside the disk are visible as illustrated in figure 2.3. The nodes are areas of high intensities and correspond to maxima of the absolute value of the electric field. Thus, the number of nodes is twice the number of wavelengths that fits into the inside of the disk denoted as the mode number of the Whispering gallery mode. The mode number is given by

$$N = \frac{nodes}{2} \tag{2.16}$$

where the *nodes* is displayed in the plotted images.

We can set up a quantization rule (Brandsrud 2015; Kokhanovsky 2011) that shows relates the refractive index of the disk, the resonance wavelength, the mode number and the length of the ray trapped inside the disk. It is given by

$$N = \frac{l_{geo}\, n}{\lambda_r}\,, \qquad N \in \mathbb{N} \tag{2.17}$$

where λ_r is the wavelength of the trapped mode, *n* the refractive index of the disk, *N* the mode number and l_{geo} the geometrical length of the ray, i.e. the actual length of the ray that travels along the surface of the disk. When *N* becomes very high, the geometrical length approaches the circumferences of the disk, given as $\lim\limits_{N\to\infty} l_{geo} = 2\pi r$.
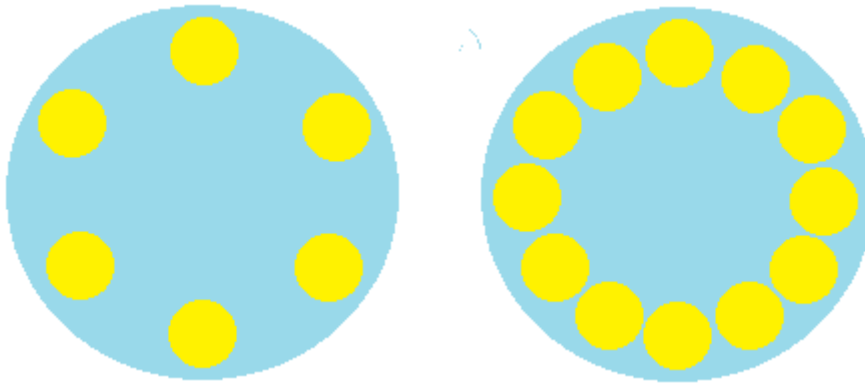

Figure 2.3: Whispering gallery modes occurs at specific wavelengths. Inside the disk bright nodes arranged in a regular order appears which corresponds to maxima of the absolute value of the electric field. In the disk to the left 6 nodes appear, which corresponds to 3 wavelengths inside the disk (N=3). The disk to the left contains 12 nodes and therefore 6 wavelengths (N=6) is trapped inside the disk.

In order to find a geometrical length for smaller values of N. The length of the ray that bounces inside the disk can be compared with the circumference of a N-sided polygon inscribed in a circle, showed in figure 2.4 and given by

$$l_{poly} = 2N \, sin\left(\frac{\pi}{N}\right) r \qquad (2.18)$$

where N is the mode number and r is the radius to the disk. Notice that for this thesis the
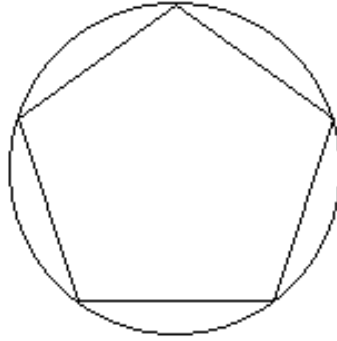

Figure 2.4: A 5-sided polygon inscribed in a circle.

polygon length is approximated for a N-sided polygon and not a polygon with sides equal to the number of nodes.

Solving equations (2.17) and (2.18) for the radius we obtain the radius of a circle that frame the polygonal whispering gallery ray, given as

$$\hat{R} = \frac{\lambda_r}{2 \sin\left(\frac{\pi}{N}\right) n} \qquad (2.19)$$

where is the resonant wavelength, λ_r with the corresponding mode number N and n is the refractive index to the disk.

2.5 Grid resolution

In this thesis, we refer to the grid resolution as the number of lattice points used in *x*- and *y*-direction for the square framing the disk. This is illustrated in figure 2.5, where a grid resolution of 8x8 lattice points is shown.
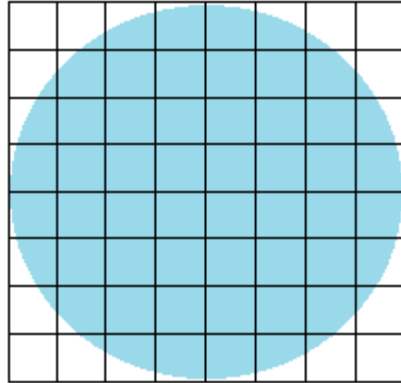

Figure 2.5: The disk with a square framing the disk. The square is discretize into a lattice structure with grid resolution of 8x8 lattice points.

Later we will show plots where the squared absolute value of the wave function $\left|\vec{\Psi}_j\right|^2$ is calculated at every lattice point.

3 Methods

3.1 Analytical plane wave scattering method

We consider a plane wave that impinges at a "soft disk". As shown in figure 3.1, the soft disk is characterized by a constant potential $V = V_0$ inside the disk and the potential outside the disk is zero. In order to calculate solutions of the wave function for the problem of a plane wave scattering at a soft disk in two dimensions, we used the analytical solutions for the problem described in lecture notes of Reinhold Blümel from June 26, 2012.
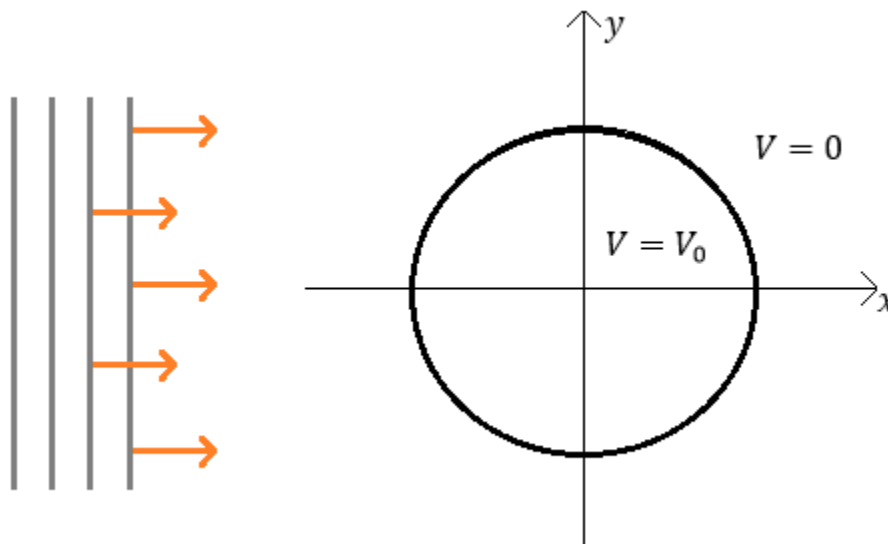

Figure 3.1: The plane wave is moving in the positive x-direction against the disk with a constant potential inside.

In order to solve the problem analytically, we have to solve the Helmholtz equation in equation (2.15). Since $n = 1$ outside the disk and $n > 1$ inside the disk, we define the wavenumber inside the disk as

$$\kappa = kn \qquad (3.1)$$

where *n* is the refractive index to the disk.

The radial distance from origin is denoted by r and for the radius of the disk is expressed by a. Outside the disk i.e. $r > a$, the potential is zero. The ansatz for the wave function outside the disk is as follows

$$\Psi_{\text{out}}(r, \theta) = \sum_{l=-\infty}^{+\infty} i^l J_l(kr)e^{il\theta} + \sum_{l=-\infty}^{+\infty} A_l H_l^{(+)}(kr)e^{il\theta} \tag{3.2}$$

where the first term represents the incoming plane wave in the plane wave expansion with Bessel functions of first kind J_l of order l and the second term is presented as a superposition of outgoing wave spherical waves represented by Hankel functions $H_l^{(+)}$ of first kind of order l with expansion parameters A_l. The polar angle is denoted by θ.

Inside the disk, i.e. $r < a$, the wave function is given by

$$\Psi_{\text{in}}(r, \theta) = \sum_{l=-\infty}^{+\infty} B_l J_l(\kappa r)\, e^{il\theta} \tag{3.3}$$

where the functions J_l are the Bessel function of first kind of order l. The parameters A_l and B_l are determined by boundary conditions. Since the Helmholtz equation is a second-order differential equation, the wave function its first derivative have to be continuous everywhere, including at the boundary between the region outside the disk and inside the disk. Therefore it follow:

$$i^l J_l(ka) + A_l H_l^{(+)}(ka) = B_l J_l(\kappa a) \tag{3.4}$$

$$i^l k J_l'(ka) + A_l k H_l^{(+)'}(ka) = B_l \kappa J_l'(\kappa a) \tag{3.5}$$

where equation (3.4) represent the condition for continuity of the wave function at the boundary of the disk, while equation (3.5) represented the condition for continuity at the first derivative of the wave function.

Solving equations (3.4) and (3.5) for the parameters A_l and B_l we obtain

$$A_l = \frac{i^l [J_l'(ka)\, J(\kappa a) - n\, J_l'(\kappa a)\, J_l(ka)]}{n\, J_l'(\kappa a) H_l^{(+)}(ka) - H_l^{(+)'}(ka)\, J_l(\kappa a)} \qquad (3.6)$$

and

$$B_l = \frac{i^l [H_l^{(+)'}(ka)\, J_l(ka) - J_l'(ka) H_l^{(+)}(ka)]}{H_l^{(+)'}(ka)\, J_l(\kappa a) - n\, J_l'(\kappa a) H_l^{(+)}(ka)} \qquad (3.7)$$

For the calculation of derivatives of Bessel and Hankel functions we used recurrence relations as given in (Abramowitz & Stegun 1972).

The method described in this section is implemented as an algorithm in MATLAB by the author of this thesis. This program is presented as *ProgramIII.m* in Appendix A. From now on, this script is called program III.

3.1.1   Program III

For each wavenumber, the following parameters can be changed in program III.

- Radius of the disk.
- Refractive index of the disk.
- Pixel resolution.
- The frame outside the disk.
- The minimum and the maximum order in the plane wave expansion.

3.2 Numerical plane wave scatter algorithm

To solve the problem of the scattering of a two dimensional plane wave at one or more disks, the Green's function method was used (Green 1828). Achim Kohler and Reinhold Blümel developed the method, called the plane wave scatter algorithm (Brandsrud 2015). The algorithm uses the Lippmann-Schwinger equation and solves it numerically by discretizing the equation in a lattice structure.

We consider a system with multiple disks. The time-independent wave equation in equation (2.15) needs to be fulfilled for the area outside the disks and the area inside the disks

$$Outside: (\Delta + k^2)\Psi(\vec{r}) = 0 \tag{3.8}$$

$$Inside: (\Delta + \kappa^2)\Psi(\vec{r}) = 0 \tag{3.9}$$

where $\Psi(\vec{r})$ is the wave function and $\vec{r}$ is the position vector. In the area surrounding the disk we assume that the plane wave travels in free space, therefore the refractive index is equal to one and the angular wavenumber is k. As n is the refractive index of the disks the angular wavenumber inside the disk is $\kappa = kn$.

This type of problem can be solved with the Lippmann-Schwinger equation (Sharma & Sommerford 2006), given as

$$\Psi(\vec{r}) = \varphi(\vec{r}) - \int G(\vec{r}, \vec{r}', k) V(\vec{r}') \Psi(\vec{r}') d^2 \vec{r}' \tag{3.10}$$

where $\Psi(\vec{r})$ is the solution to the wave function in the potential $V(\vec{r}')$, $\varphi(\vec{r}')$ is the incoming wave, thus representing a solution of the free Schrödinger equation, $\vec{r}'$ is the position vector of the source point and $G(\vec{r}, \vec{r}', k)$ is Green's function.

In order to prove that $\Psi(\vec{r})$ is a solution for the wave function in the potential $V(\vec{r}')$, we apply the Helmholtz operator, $(\Delta + k^2)$ on the Lippmann-Schwinger in equation (3.10). We use that Helmholtz operator applied on Green's function gives

$$(\Delta + k^2)G(\vec{r}, \vec{r}', k) = -\delta(\vec{r} - \vec{r}') \tag{3.11}$$

where $\delta(\vec{r} - \vec{r}')$ is the delta Dirac function.

We use further that $\varphi(\vec{r})$ is a solution for the free Helmholtz equation:

$$(\Delta + k^2)\varphi(\vec{r}) = 0 \tag{3.12}$$

thus we obtain from (3.10) becomes

$$(\Delta + k^2)\Psi(\vec{r}) = \int \delta(\vec{r} - \vec{r}')V(\vec{r}')\Psi(\vec{r}')d^2\vec{r}' \tag{3.13}$$

Solving the integral and rearranging equation (3.13) and after some rearranging, we obtain

$$[-\Delta + V(\vec{r})]\,\Psi(\vec{r}) = k^2\Psi(\vec{r}) \tag{3.14}$$

where the potential of the system, $V(\vec{r})$ is given by

$$V(\vec{r}) = k^2 v(\vec{r}) \tag{3.15}$$

with $v(\vec{r})$

$$v(\vec{r}) = \begin{cases} 1 - n, & inside\ the\ disk \\ 0, & outside\ the\ disk \end{cases} \tag{3.16}$$

Thus, we have shown that equation (3.10) is equivalent to equation (3.14). Notice that the disk referred to above is homogenous with a constant refractive index.

The solution for the Green's equation defined by equation (3.11) is given as

$$G(\vec{r}, \vec{r}', k) = \frac{i}{4}H_0^{(+)}(k|\vec{r}' - \vec{r}|) \tag{3.17}$$

where $H_0^{(+)}$ is the Hankel function of the first kind of zero order, given by

$$H_0^{(+)}(x) = J_0(x) + iY_0(x) \tag{3.18}$$

where $J_0(x)$ and $Y_0(x)$ is the Bessel function of respectively the first and the second kind of zero order. We use equation (3.17) together with the expression for the plane wave from equation (2.8), which leads to the equation

$$\Psi(\vec{r}) = e^{i\vec{k}\vec{r}} - i\frac{k^2}{4}\int H_0^{(+)}(k|\vec{r}' - \vec{r}|)\ v(\vec{r}')\Psi(\vec{r}')d^2\vec{r}' \tag{3.19}$$

To implement equation (3.19) numerically, the two-dimensional plane with the disks can be discretised into a lattice structure with N number of squares and square area ΔA.

The equation (3.19) is discretized on this lattice according to

$$\Psi(\vec{r_j}) = e^{i\vec{k}\vec{r_j}} - i\frac{k^2}{4}\sum_{m=1}^{N} H_0^{(+)}\left(k|\vec{r_m} - \vec{r_j}|\right) v(\vec{r_m})\Psi(\vec{r_m})\Delta A \qquad (3.20)$$

where the continuous position vectors are replaced with discrete position vectors, i.e. $\vec{r}' \to \vec{r_m}$ and $\vec{r} \to \vec{r_j}$. We denote by N_x the number of squares in x-direction, and by N_y the number of squares in y-direction. The total number of squares is then given by $N = N_x \cdot N_y$. We write the identity matrix as $I_{j,m}$ and obtain

$$\Psi_j = I_{j,m}\Psi_m = e^{i\vec{k}\vec{r_j}} - i\frac{k^2}{4}\,\Delta A\, G_{j,m}v_m\Psi_m \qquad (3.21)$$

We write this in matrix notation

$$\mathbf{M}\vec{\Psi} = \vec{R} \qquad (3.22)$$

where $\vec{R}$ is defined as

$$R = \begin{pmatrix} e^{i\vec{k}\vec{r_1}} \\ \vdots \\ e^{i\vec{k}\vec{r_j}} \end{pmatrix} \qquad (3.23)$$

The matrix $\mathbf{M}$ is given by

$$\mathbf{M} = \mathbf{I} + i\frac{k^2\Delta A}{4}\,\widetilde{\mathbf{G}} \qquad (3.24)$$

where every element in the matrix $\widetilde{\mathbf{G}}$ is given by

$$\widetilde{G} = G_{j,m}v_m \qquad (3.25)$$

The algorithm was implemented in MATLAB by Achim Kohler and Reinhold Blümel, as the script *Disk_Scattering20082015.m,* which can be found in M.A Brandsrud master thesis. Rozalia Lucaks vectorised the program as *Disk_Scattering20082015vec.m* presented in Appendix B. From now on, this script is called program I.

3.2.1 Program I

For each wavenumber, the following parameters can be change in program I.

- The amount of disks in x- and y-direction.
- Radius of the disks.
- Refractive index of the disks.
- Grid resolution, i.e. the number of squares in the lattice structure in *x*- and *y*-direction.
- Angle of incidence for the incoming plane wave.

Greens function has a singularity at the zero argument. A simplification that were done in the program is that the Greens function were set to zero at a zero argument.

3.3 Analytical spherical wave scattering method

For a spherical wave that impinges on a disk with constant potential, an exact analytical
solution can be found. For the derivation of the exact solutions, lecture notes of Reinhold
Blümel were used. For this special the radially symmetric and constant potential is given by

$$v(\vec{r}) = \begin{cases} v_0 & if\ r \leq R \\ 0 & if\ r \geq R \end{cases} \tag{3.26}$$

where R is the radius of the disk and r is the radial distance from the origin of the disk. The
constant potential inside the disk, v_0 can be written as

$$v_0 = 1 - n^2 \tag{3.27}$$

where n is the refractive index of the disk. The angular wavenumber outside the disk is k and
the angular wavenumber inside the disk is defined as

$$\beta = \sqrt{k^2 - v_o} = kn \tag{3.28}$$

A solution for the Helmholtz equation in equation (2.15) inside the disk is given by

$$\psi_{in}(r) = A_m(k)J_m(\beta r)e^{im\theta} \tag{3.29}$$

where $A_m(k)$ is not yet specified constant, J_m is the Bessel function of first kind of order
m and θ is the polar angle. In the space outside the disk, the potential is equal to zero. We
write the solution to equation (2.15) in the form of a superposition of an incoming wave and a
scattered, outgoing wave according to

$$\psi_{out}(r) = H_m^{(-)}(kr)e^{im\theta} + S_m(k)H_m^{(+)}(kr)e^{im\theta} \tag{3.30}$$

where and $S_m(k)$ defines the diagonal elements of the scatter matrix, which is a diagonal
matrix. $H_m^{(+)}$ and $H_m^{(-)}$ are the Hankel functions of the first and second kind of m order,
respectively and are given by

$$H_m^{(\pm)} = J_m(kr) \pm iY_m(kr) \tag{3.31}$$

where Y_m is the Bessel function of the second kind of order m. The elements $S_m(k)$ can be
found by the use of boundary conditions.

We require that the wave functions ψ_{in} and ψ_{out} and their derivatives are continuous at the boundary of the disk boundary. Thus, we obtain the following two conditions

$$A_m(k)J_m(\beta R) = H_m^{(-)}(kR) + S_m(k)H_m^{(+)}(kR) \tag{3.32}$$

$$A_m(k)\beta J_m'(\beta R) = k\left[H_m^{(-)'}(kR) + S_m(k)H_m^{(+)'}(kR)\right] \tag{3.33}$$

Solving equations (3.32) and (3.33) for $S_m(k)$, we obtain

$$S_m(k) = \frac{n\,J_m'(\beta R)H_m^{(-)}(kR) - H_m^{(-)'}(kR)J_m(\beta R)}{J_m(\beta R)H_m^{(+)'}(kR) - n\,J_m'(\beta R)H_m^{(+)}(kR)} \tag{3.34}$$

Two properties of (3.34) are immediately apparent:

i) Since the numerator is the complex conjugate of the denominator, $S_m(k)$ is a pure phase with absolute magnitude equal to 1.

ii) For $v_0 = 0$, which implies $\beta = k$, we see immediately that $S_m(k) = 1$. This is the expected results since it follows that

$\psi_{out}(r) = \left[H_m^{(-)}(kr) + H_m^{(+)}(kr)\right]e^{im\theta}$. Thus, $\psi_{in}(r) = \psi_{out}(r)$, since

$J_m(kr) = \left[H_m^{(-)}(kr) + H_m^{(+)}(kr)\right]/2$.

Since $S_m(k)$ is a pure phase, we define the scattering phase shift $\delta_m(k)$ according to

$$S_m(k) = e^{2i\delta_m(k)} \tag{3.35}$$

The parameter $A_m(k)$ can be obtained by solving equations (3.32) and (3.33) for $A_m(k)$. We obtain

$$A_m(k) = \frac{H_m^{(+)}(kR)H_m^{(-)'}(kR) + H_m^{(-)}(kR)H_m^{(+)'}(kR)}{n\,J_m'(\beta R)H_m^{(+)}(kR) - H_m^{(+)'}(kR)J_m(\beta R)} \tag{3.36}$$

For the calculation of derivatives of Bessel and Hankel functions we used recurrence relations for Bessel functions (Abramowitz & Stegun 1972).

The algorithm was implemented in MATLAB by the author of this thesis. This program is presented as *SpericalWave_Scattering.m* in Appendix C. From now on, this script is called program II.

3.3.1 Program II

In order to test program, the two properties described under section 3.3 as i) and ii) were checked to hold.

For each wavenumber, the following parameters can be change in program II.

- Radius of the disk.
- Refractive index of the disk.
- Pixel resolution.

4 Results and discussion

4.1 Program based on analytical solution for plane wave scattering (program III)

In the following we evaluate the analytical program of the scattering of a plane wave at a single disk (MATLAB script *ProgramIII.m,* called program III), described in section 3.1. In figure 4.1 the integral of the squared absolute value of the wave function $\left|\vec{\Psi}\right|^{2}$ over a square covering the disk is plotted for the wavenumber region from $500\ cm^{-1}$ to $1400\ cm^{-1}$ for the analytical plane wave scattering at a disk (program III). The integration was done by discretizing a square that just covers the disk into 200 grid point in both *x*- and *y*- direction and calculating the intensity at every element $\left|\vec{\Psi}_{j}\right|^{2}$. As radius of the disk and as refractive index $R=10\ \mu m$ and $n=1.9$ were chosen, respectively. In figure 4.1, nine distinct peaks appear at nine different wavenumbers. The nine images corresponding to the nine peak wavenumber are displayed in the same figure. As long as not stated otherwise, the color intensity scale for the wave function plots was autoscaled in MATLAB. Because the solution is analytical, the simulations were not very time consuming, and could be done on the author's computer.
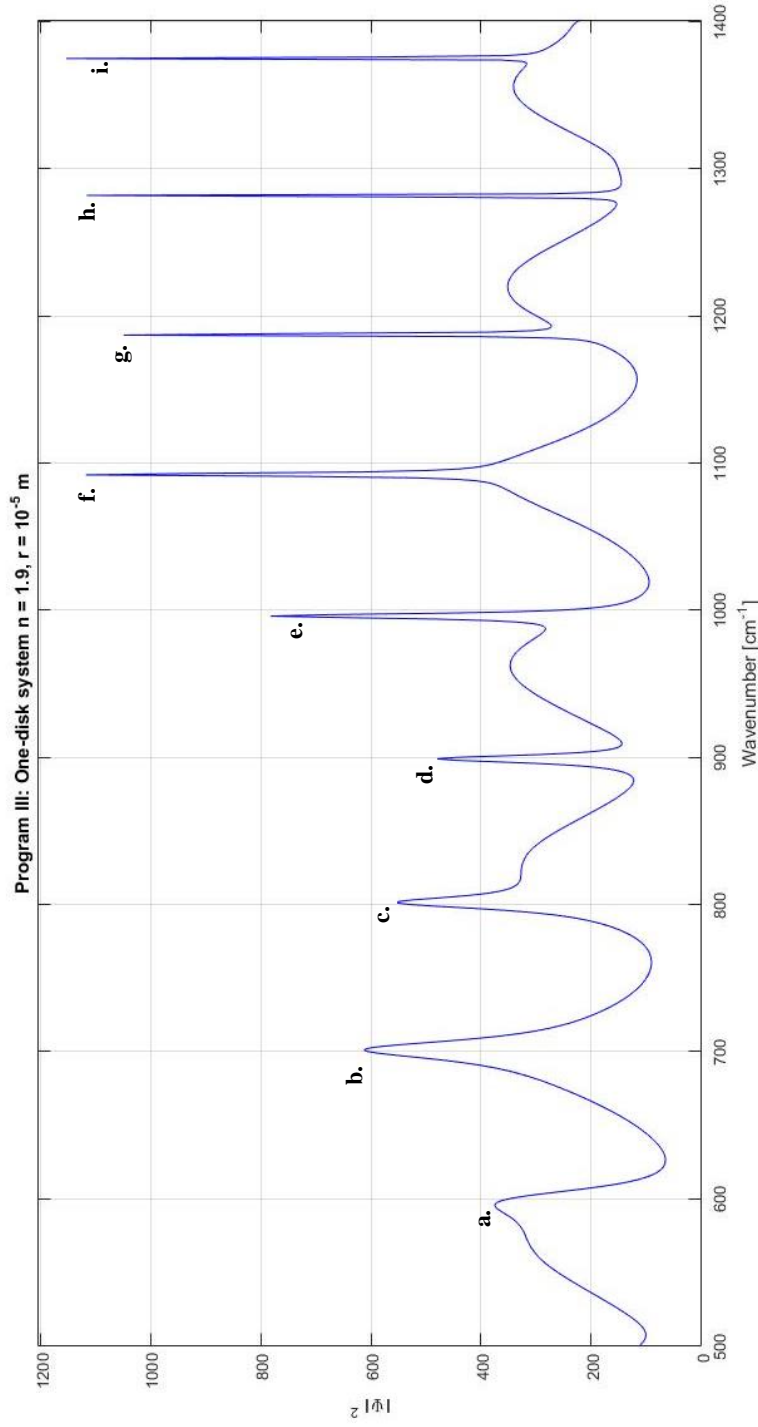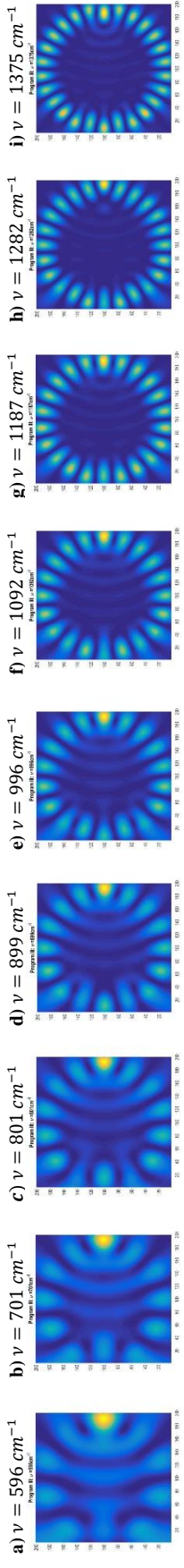
a) $v = 596\ cm^{-1}$

b) $v = 701\ cm^{-1}$

c) $v = 801\ cm^{-1}$

d) $v = 899\ cm^{-1}$

e) $v = 996\ cm^{-1}$

f) $v = 1092\ cm^{-1}$

g) $v = 1187\ cm^{-1}$

h) $v = 1282\ cm^{-1}$

i) $v = 1375\ cm^{-1}$

Program III: One-disk system n = 1.9, r = 10^{-5} m

Figure 4.1: The integral of the squared absolute value of the wave function $|\Psi|^2$ is plotted as a function of the wavenumber v, for a plane wave coming from the left and impinging at a disk with 10 µm and a refractive index of 1.9. For the calculation of the wave function, the analytical solutions for the plane wave scattering (program III) were used. The graph shows nine distinct peaks a. to i. and each peak correspond to wave function plots in figure a) to i).

The peak in the graph figure 4.1 correspond to maxima in the total intensity of the wave function and represent resonances at the nine wavelengths. The images of the resonance wavenumbers show the typical pattern of Whispering galley modes. The displayed pattern shows a ring of nodes. The number of nodes is approximately twice the number of wavelengths that fit along the inside of the boundary of the disk as illustrated below. At the first peak, $\nu = 596\ cm^{-1}$, 10 nodes appear as shown in the wave function plot in figure 4.2. These correspond to five wavelengths that fit into the inside of the disk as a standing wave that is located at the inside of the boundary. We defined the number of wavenumbers fitting into the disk as the mode number of the Whispering gallery mode. The mode number of the Whispering gallery mode in figure 4.2 is $N = 5$ from equation (2.16).
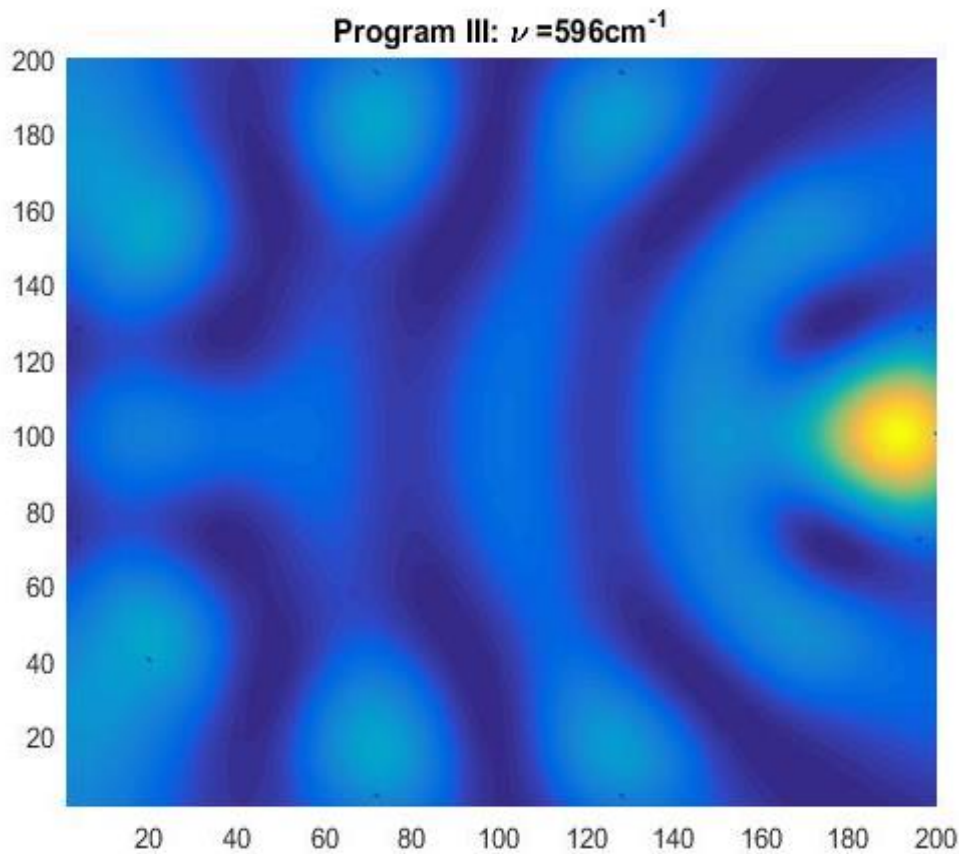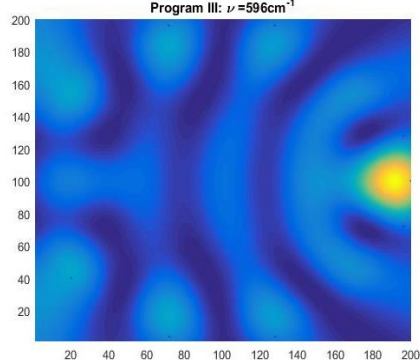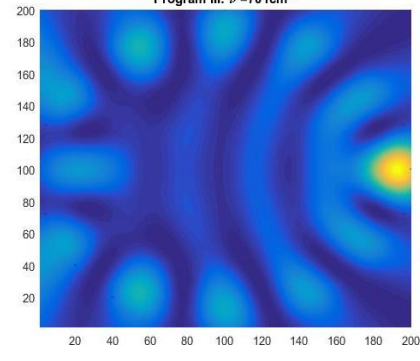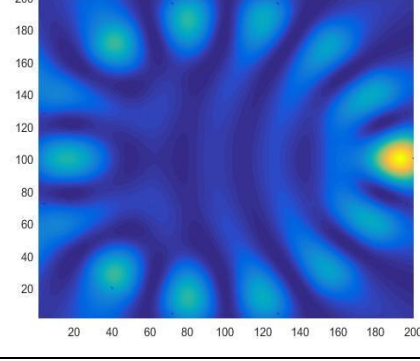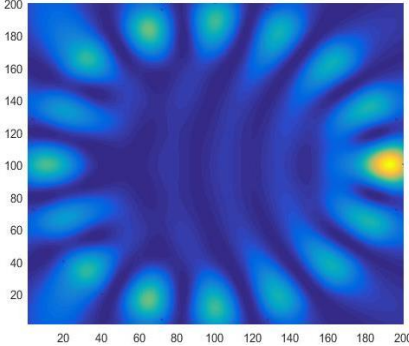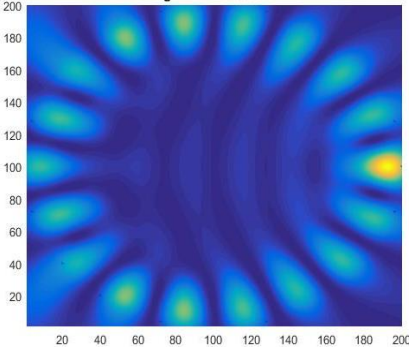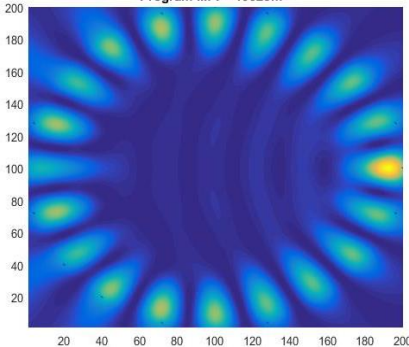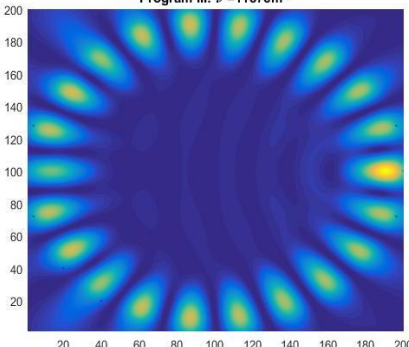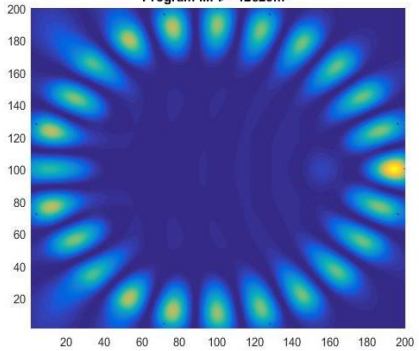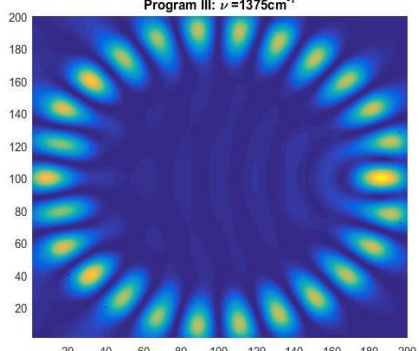
Figure 4.2: The squared absolute value of the wave function is plotted. The wave function corresponds to a Whispering gallery mode displaying 10 nodes that correspond to five wavelengths inside the disk. The plotted region covers the disk exactly. At the axes, the grid pixel number used for the plotting is shown.

At the following peaks, e.g. higher wavenumber, the nodes increased with two nodes for every peak. At the last peak $\nu = 1375 \ cm^{-1}$ 26 nodes were counted. This corresponds to mode numbers ranging from N=5 to $N = 13$, as shown in table 4.1. This result shows that the program III is highly stable and therefore a good confirmation that the method was successfully implemented as an algorithm.

Table 4.1: The table shows the wavenumber positions and the wave function plots for the resonances in figure 4.1. The nodes in the wave function is counted and displayed in the second column and the mode number in third column is calculated with equation.(2.16).

Wavenumber	Nodes	N	
596 cm^{-1}	10	5	
701 cm^{-1}	12	6	
801 cm^{-1}	14	7	

899 cm^{-1}	16	8	
996 cm^{-1}	18	9	
1092 cm^{-1}	20	10	
1187 cm^{-1}	22	11	

1282 cm^{-1}	24	12	
1375 cm^{-1}	26	13	

26

The quantization rule of equation (2.17) shows the mathematical relationship between the refractive index of the disk, the resonance wavelength, the mode number and the geometrical length of the ray that corresponds with Whispering gallery resonances. In order to test the quantization rule of equation (2.17), we calculated the length of corresponding polygonal whispering gallery rays as illustrated in figure 2.4 for each Whispering gallery mode shown in table 4.1. At each resonance, the resonance wavelength was calculated as $\lambda_r = \frac{1}{v_r}$. Equation (2.19) was used to calculate $\hat{R}$, which is the radius of a circle that frame the corresponding polygonal whispering gallery ray. The result is shown in table 4.2. The calculated radius $\hat{R}$ is further compared to the actual radius of the disk R by calculating the difference between $\hat{R}$ and R. In addition, the geometrical length of the polygonal ray, $\hat{l}$ calculated according to equation (2.18) is presented. Notice that the mode number, N is equivalent to the mode number calculated by the quantization rule of equation (2.17) using the geometrical length $\hat{l}$.

Table 4.2: The table shows the wavenumber and mode number for the Whispering gallery resonances from table 4.1. Notice that the mode number, N is equivalent to the mode number calculated by the quantization rule of equation (2.17) using the geometrical length $\hat{l}$. The calculated radius $\hat{R}$ is the radius of a circle that frame the polygon whispering gallery ray, calculated according to equation (2.19). The calculated radius $\hat{R}$ is compared to the actual radius of the disk R by $R - \hat{R}$ where $R = 10\,\mu m$. The geometrical length $\hat{l}$ is the length of polygonal ray inside the disk, calculated according to equation (2.18). The geometrical length of the polygonal ray $\hat{l}$ is compare to the circumference of the disk $2\pi R$, where $2\pi R = 62,8\,\mu m$.

$Wavenumber, v_r$ $[cm^{-1}]$	N	$\hat{R}$ $[\mu m]$	$R - \hat{R}$ $R = 10.0\,\mu m$	$\hat{l}$ $[\mu m]$	$2\pi R - \hat{l}$ $2\pi R = 62.8\,\mu m$
596	5	7.51	2.49	44.2	18.7
701	6	7.51	2.49	45.0	17.8
801	7	7.57	2.43	46.0	16.8
899	8	7.65	2.35	46.8	16.0
996	9	7.73	2.27	47.6	15.3
1092	10	7.80	2.20	48.2	14.6
1187	11	7.87	2.13	48.8	14.1
1282	12	7.93	2.07	49.3	13.6
1375	13	8.00	2.00	49.8	13.1

Another way to test the quantization rule in equation (2.17) is to use the approximation that for a high mode number the geometrical length of the polygonal ray is approximately the circumference of the disk. The geometrical length calculated as circumference of a N-sided polygon inscribed in the disk, l_{poly} according to equation (2.18) is presented in table 4.3. In

addition, the table presents the mode number N_{poly} calculated from quantization rule in equation (2.17) with l_{poly} as the geometrical length.

Table 4.3: The table shows the wavenumber and mode number for the Whispering gallery modes from table 4.1. The geometrical length, l_{poly} is calculated according to equation. (2.18) as the circumference of a polygon inscribed inside the disk. The geometrical length L_{poly} is compare to the circumference of the disk $2\pi R$, where $2\pi R = 62.8\ \mu m$. The mode number N_{poly} is calculated from quantization rule in equation. (2.17) with l_{poly} as the geometrical length.

Wavenumber [cm^{-1}]	N	l_{poly} [μm]	$2\pi R - l_{poly}$ $2\pi R = 62.8\ \mu m$	N_{poly}
596	5	58.8	4.05	6.70
701	6	60.0	2.83	8.00
801	7	60.7	2.09	9.20
899	8	61.2	1.60	10.5
996	9	61.6	1.27	11.7
1092	10	61.7	1.03	12.8
1187	11	62.0	0.85	14.0
1282	12	62.1	0.72	15.1
1375	13	62.2	0.61	16.3

From table 4.2 it is obvious that the geometrical length of the polygonal ray, $\hat{l}$ is getting closer to the circumference of the disk when the mode number increases. We can further see in table 4.3 that the geometrical length of the inscribed polygon l_{poly} also is getting closer to the disk circumference as the wavenumber increases. A comparison between the geometrical length of the polygonal ray $\hat{l}$ from table 4.2 and the circumference of a polygon inscribed in the disk l_{poly} from table 4.3 shows a large degree of difference. The mode number calculated with the quantization rule in equation (2.17) using the geometrical length of the polygonal ray $\hat{l}$ from table 4.2 gives the mode number N. A comparison between the mode number N in table 4.2 and the mode number N_{poly} from table 4.3 calculated with the quantization rule in equation (2.17) with circumference of a polygon inscribed in the disk l_{poly} (table 4.3), also shows a large degree of disagreement. Hence, the circumference of an inscribed polygon l_{poly}, is not a good approximation for the geometrical length for a mode number up to $N = 13$.

Furthermore, it is interesting to see if the pixel resolution changes the characteristics of the wave function plots. Figure 4.3 show plots of the absolute value of the wave function for the

whispering gallery mode corresponding to the peak at 801 μm in figure 4.1c using a grid pixel resolution of 50x50 and 200x200, in (a) and (b), respectively.
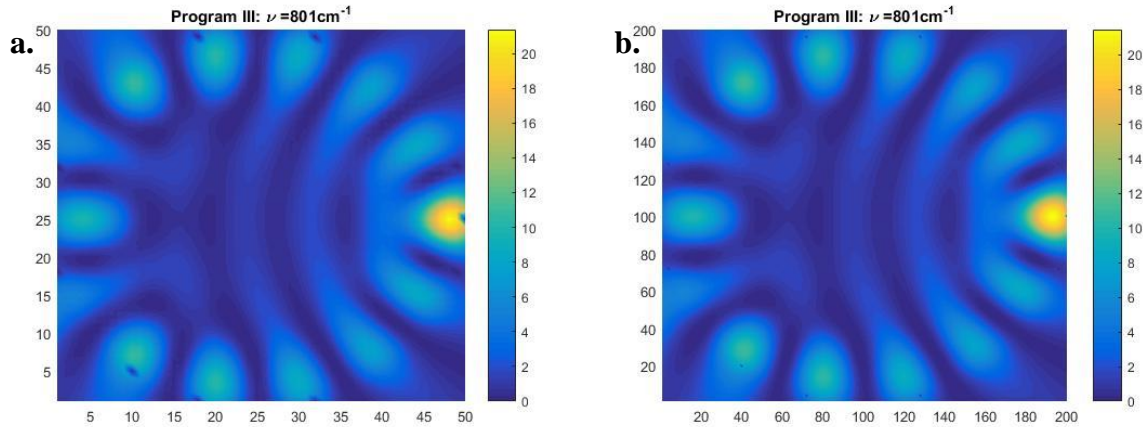

Figure 4.3: Two wave function plots for the Whispering gallery mode corresponding to the peak found at 801 cm^{-1} in figure 4.1. At right side of the plots, a colorbar with the range of intensity values 0 to 20 is displayed. At the axes, the grid point number used for the plotting is shown. a) shows the wave function plot with pixel resolution 50x50 and b) shows the wave function plot with pixel resolution 200x200.

Visually the two wave function plots are very similar, except dark spots that appear in the plot with the lower pixel resolution of 50x50. The colorbars, had similar color intensity scales (0-20) for both wave function plots (a) and (b) in figure 4.3. We further investigated the wavenumber position of the resonances in the plot of the integral over the absolute value of the wave function in the square area framing the disk (graphs corresponding to the graph of figure 4.1). It turned out that the resonances appeared at the same position $\nu = 801\ cm^{-1}$ for both pixel resolutions. Thus, the pixel resolution does not seem to have a big effect on the wavenumber position where the resonance appears.

4.2 Evaluation of program based on Lippmann-Schwinger equation (program I)

In the following we evaluate the program based on the Lippmann Schwinger equation for the scattering of a plane wave at a single disk (MATLAB script *Disk_Scattering20082015vec.m* called program I) described in section 3.1. We also compare the results from the numerical algorithm based on the Lippmann Schwinger equation with the results from the plane wave scatter solution (section 4.1). The parameters chosen in this thesis is based on earlier results for a two-disk and one-disk system from M.A. Brandsrud thesis (Brandsrud 2015). The comparisons in this thesis are based on calculations done for the scattering at one disk. The disk radius is set to $R = 10\ \mu m$ and the refractive index of the disk to $n = 1.9$. Program I was used to calculate the wave function for every wavenumber in the interval $500\ cm^{-1}$ to $1400\ cm^{-1}$ for a plane wave impinging on the disk from the left. For the obtained wave functions, we calculated the integral of the squared absolute value of the wave function, $\left|\vec{\Psi}\right|^2$, over the area of the square framing the disk. The results are plotted for grid resolutions of 50x50, 75x75 and 100x100 as described in section 2.5 in figure 4.4, figure 4.5 and figure 4.6, respectively. As previously, peaks with increased total intensities appear. Plots of the absolute value of the wave functions for the peak wavenumbers are plotted in the same figure. Since the numerical calculations were very time consuming, program I was vectorised by Rozalia Lukacs which increased the speed from four hours to about 2,5 minutes for a grid resolution of 100x100. Most of the simulations were done at the compute cluster at UiT – The Arctic University, the Linux Cluster Stallo, one of the Notur hardware resources, located in Tromsø.

a) $v = 606\ cm^{-1}$

b) $v = 710\ cm^{-1}$

c) $v = 812\ cm^{-1}$

d) $v = 913\ cm^{-1}$

e) $v = 1019\ cm^{-1}$

f) $v = 1132\ cm^{-1}$

g) $v = 1241\ cm^{-1}$

h) $v = 1339\ cm^{-1}$

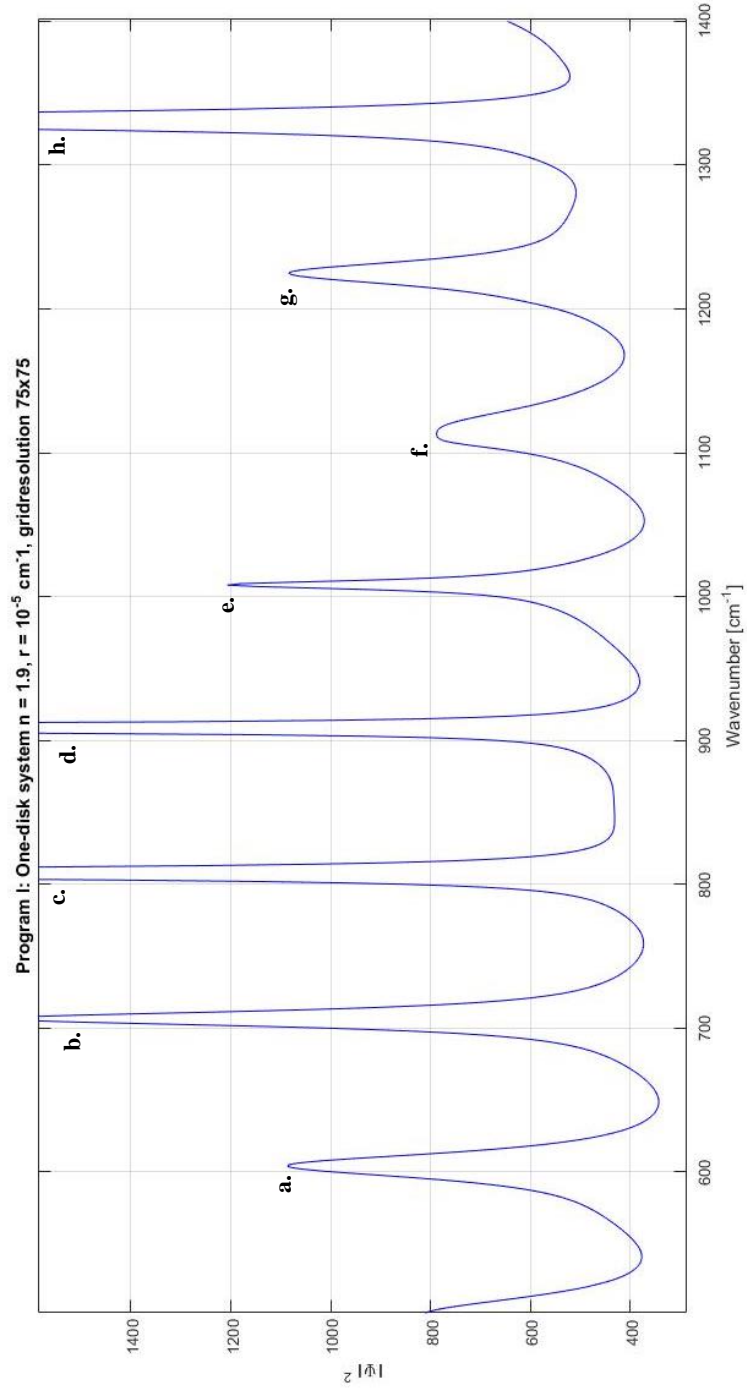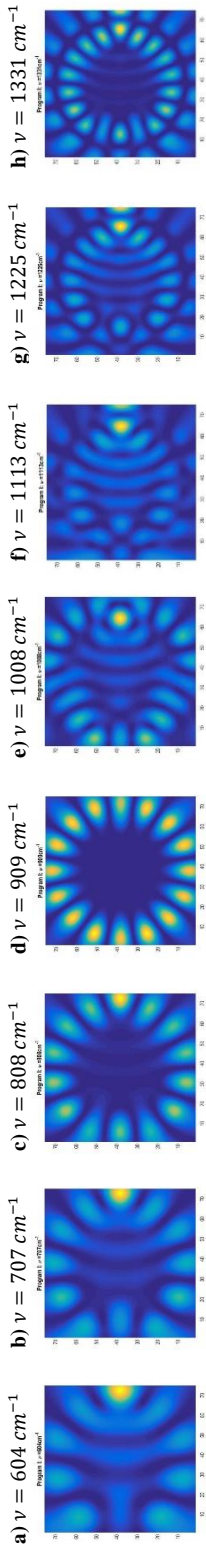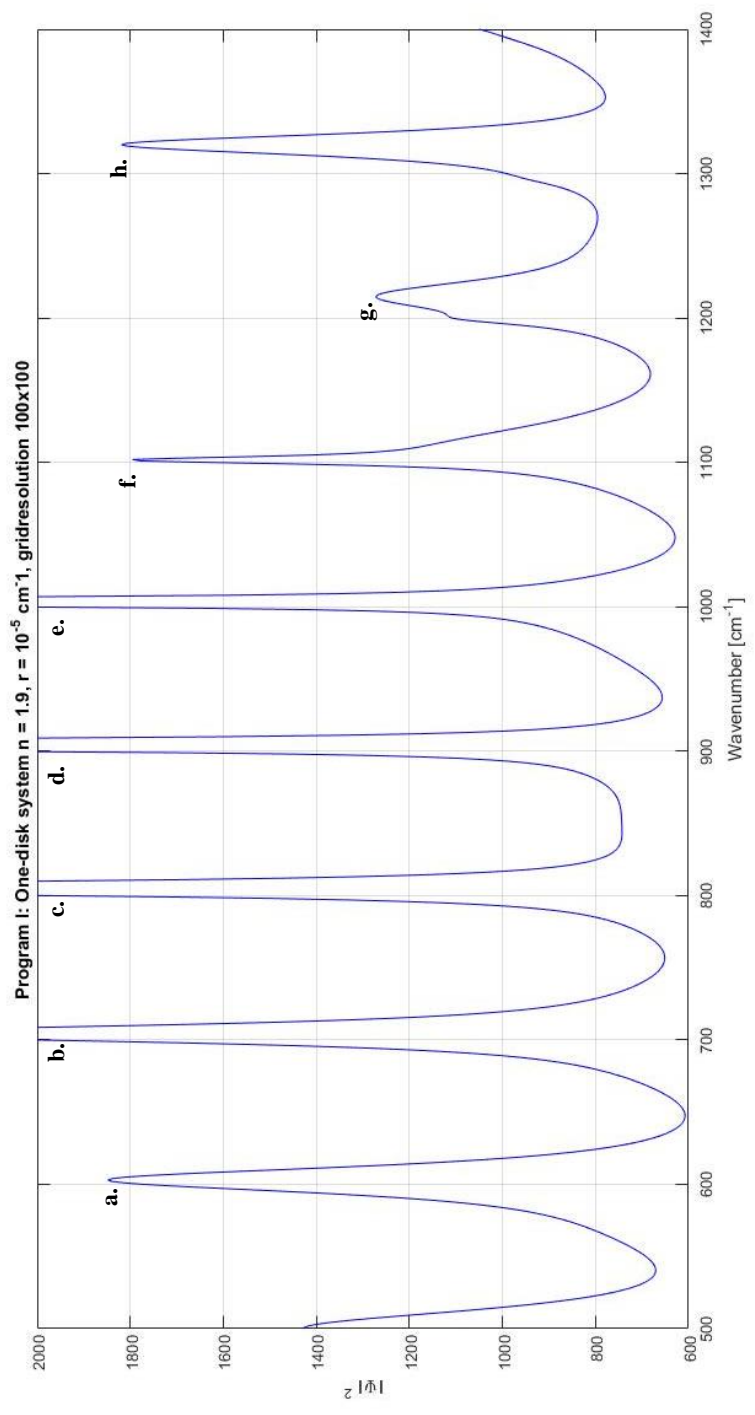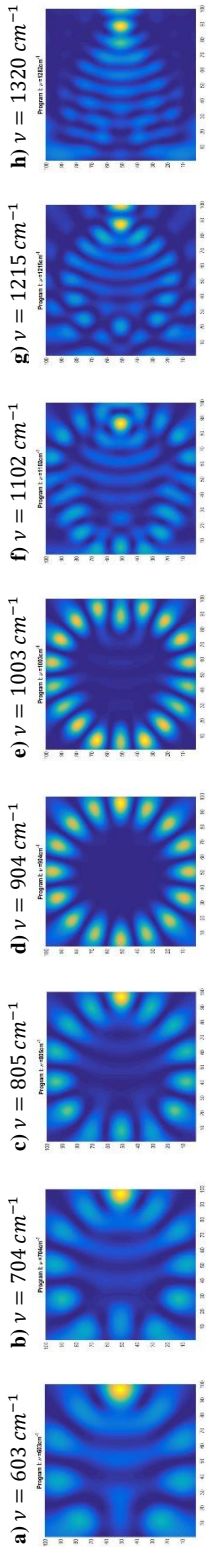Program I: One-disk system n = 1.9, r = 10⁻⁵ cm⁻1, gridsize = 50x50
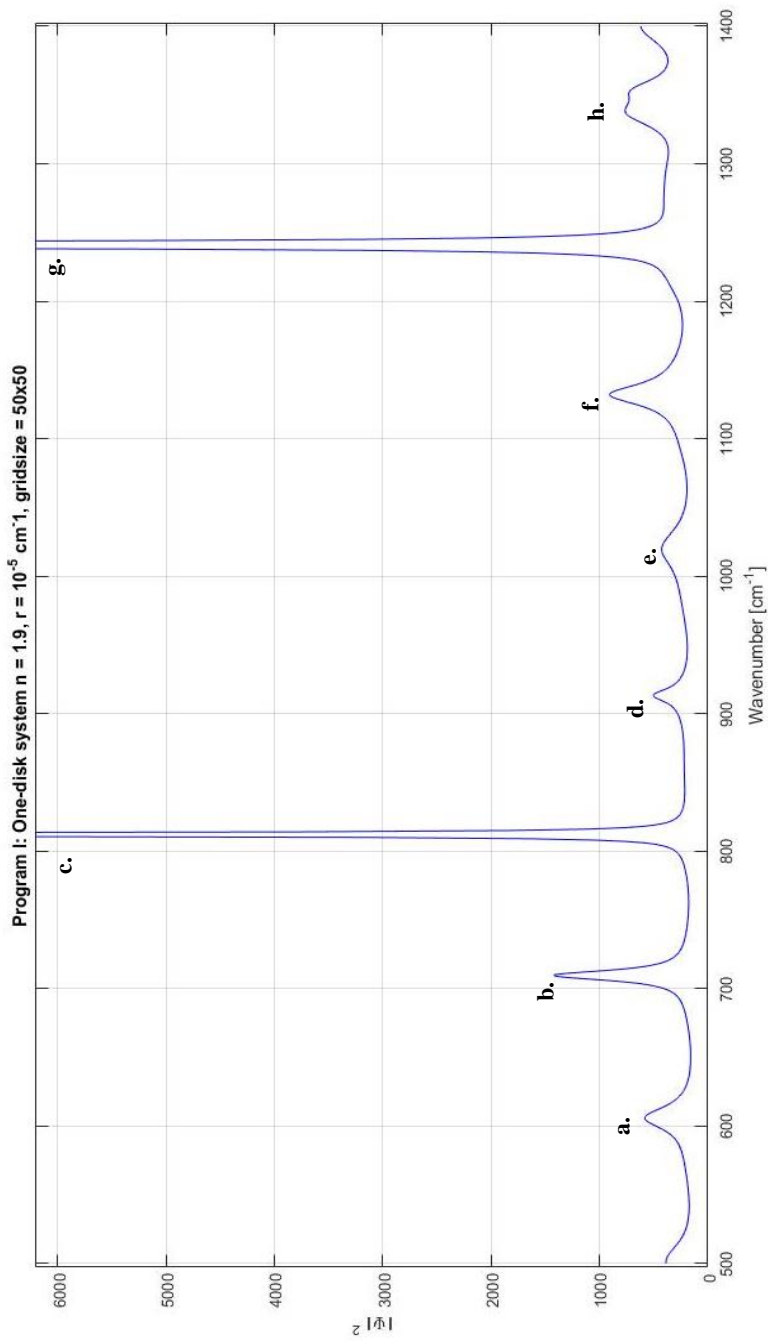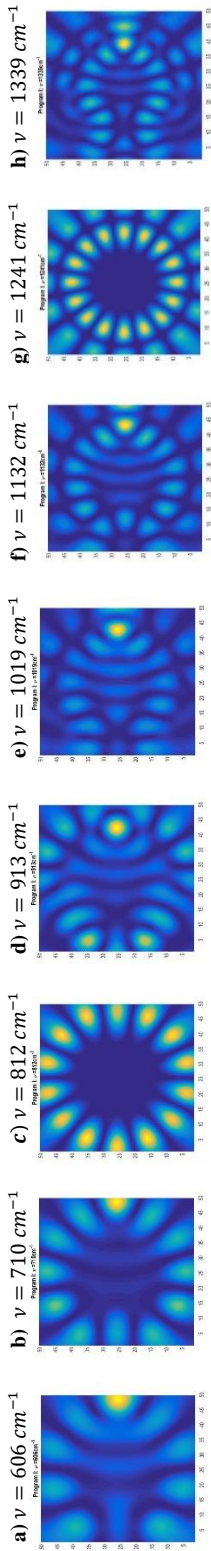
Figure 4.4: The integral of the squared absolute value of the wave function $|\Psi|^2$ is plotted as a function of the wavenumber v, for a plane wave coming from the left and impinging at a disk with 10 μm and a refractive index of 1.9. For the calculation of the wave function, the numerical solutions for the plane wave scattering (program I) were used with a grid resolution of 50x50. The graph shows eight distinct peaks a. to h. and each peak correspond to wave function plots in figure a) to h).
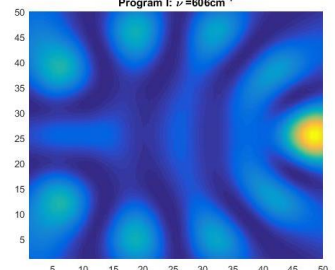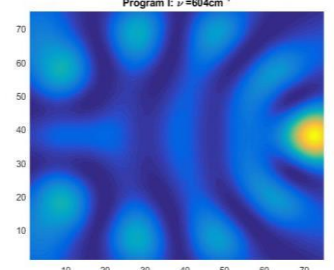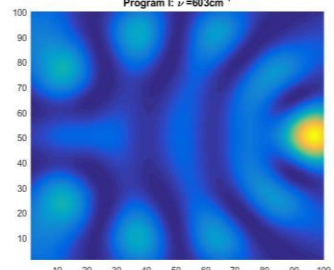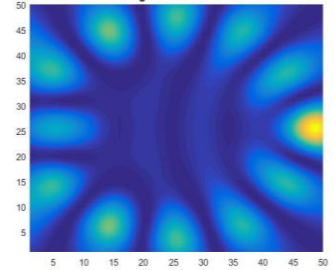
31

a) $v = 604\ cm^{-1}$ b) $v = 707\ cm^{-1}$ c) $v = 808\ cm^{-1}$ d) $v = 909\ cm^{-1}$ e) $v = 1008\ cm^{-1}$ f) $v = 1113\ cm^{-1}$ g) $v = 1225\ cm^{-1}$ h) $v = 1331\ cm^{-1}$

Figure 4.5: The integral of the squared absolute value of the wave function $|\Psi|^2$ is plotted as a function of the wavenumber v, for a plane wave coming from the left and impinging at a disk with 10 μm and a refractive index of 1.9. For the calculation of the wave function, the numerical solutions for the plane wave scattering (program I) were used with a grid resolution of 75x75. The graph shows eight distinct peaks a. to h. and each peak correspond to wave function plots in figure a) to h).

a) $v = 603\ cm^{-1}$ b) $v = 704\ cm^{-1}$ c) $v = 805\ cm^{-1}$ d) $v = 904\ cm^{-1}$ e) $v = 1003\ cm^{-1}$ f) $v = 1102\ cm^{-1}$ g) $v = 1215\ cm^{-1}$ h) $v = 1320\ cm^{-1}$

Figure 4.6: The integral of the squared absolute value of the wave function $|\Psi|^2$ is plotted as a function of the wavenumber v, for a plane wave coming from the left and impinging at a disk with 10 μm and a refractive index of 1.9. For the calculation of the wave function, the numerical solutions for the plane wave scattering (program I) were used with a grid resolution of 100x100. The graph shows eight distinct peaks a. to h. and each peak correspond to wave function plots in figure a) to h).
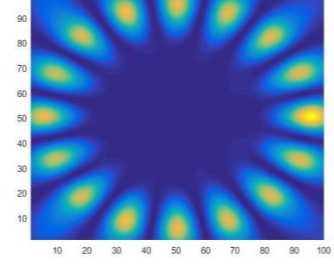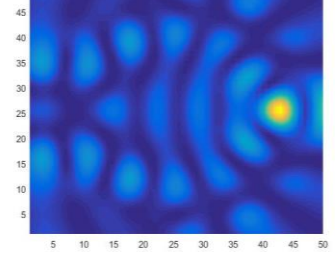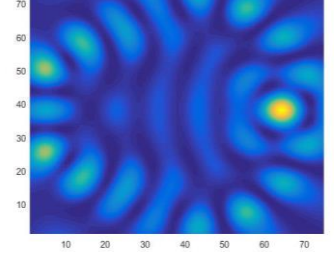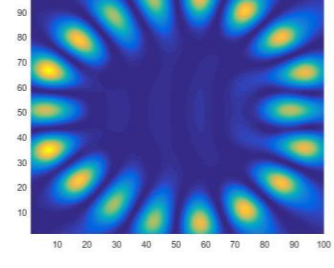
33
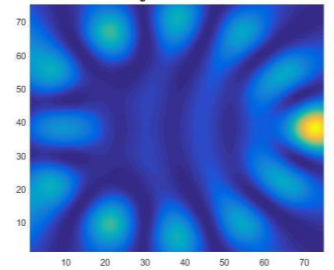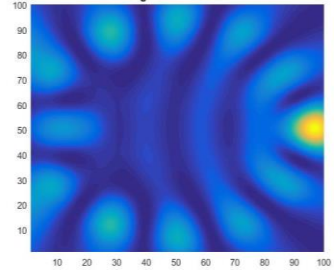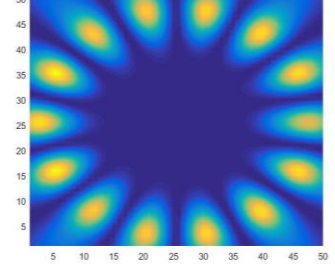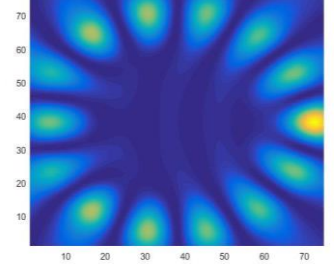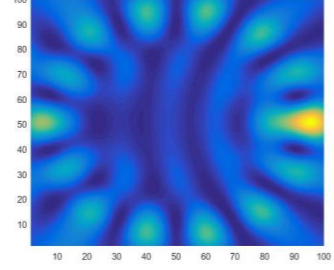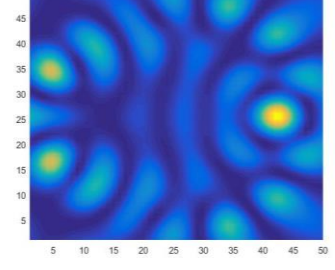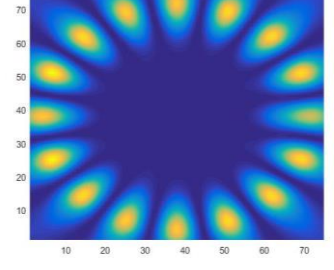
As we can see from the results in figure 4.4, figure 4.5 and figure 4.6, the numerical method used in this thesis is stable. In each of the graphs, eight distinct peaks appear and they are located in the same distance from each other. Each peak corresponds to an increase in the intensity caused by a resonance. In some of the wave function plots belonging to the first peaks with the lowest wavenumber, we can observe the typical pattern of Whispering gallery modes resonances. The nodes are areas of high intensity and as explained in section 2.4, the number of nodes is twice the number of wavelengths that fit into the inside of the disk, i.e. mode number. As the wavenumber increases, the ring of nodes that is characteristic for Whispering gallery modes cannot be observed in every wave function plot and we can therefore not conclude that the intensity increase was due to Whispering gallery resonances. As previously, we denote the modes of all resonances in figure 4.4, figure 4.5 and figure 4.6 with a mode number which is twice the number of nodes visible in the wave function plots. The wave function plots without visible nodes is given one mode number higher than the previous resonance with lower wavenumber. In table 4.4 the modes are listed according to their mode number and the wavenumber position of the resonances is given for the three grid resolutions used. The table shows that the resonances appear at almost the same wavenumbers for the three grid resolutions, while the discrepancy between the three grid resolutions increases with increasing wave numbers. For each resonance we can observe, that the resonances moves to smaller wavenumbers as the grid resolution increases. It is interesting to note that the resonances appear at almost the same distance from each other, with a displacement of 100 wavenumbers.

Table 4.4 Modes are listed according to their mode number and the wavenumber position of the resonances is given for the three grid resolutions used in program I.

Mode number	Wavenumber [cm^{-1}]		
	Grid res. 50x50	Grid res. 75x75	Grid res. 100x100
5	606	604	603
6	710	707	704
7	812	808	805
8	913	909	904
9	1019	1008	1003
10	1132	1113	1102
11	1241	1225	1215
12	1339	1331	1320

For comparison, the wave function plots (a) to (f) in figure 4.4, figure 4.5 and figure 4.6 with the corresponding mode number are plotted in table 4.5. As we can see for mode number 5, 6 and 7 the images of the wave function plots shows the typically Whispering gallery mode pattern. For mode number 8, the WGM pattern cannot be seen in the image from grid resolution of 50x50, but in the images for the two higher resolutions. This is also the case for mode number 9, where the WGM pattern appears for the grid resolution 100x100, but is not visible when a grid resolution of 50x50 and 75x75 is used. For mode number 10 and higher, the WGM pattern has disappeared for all three grid resolutions. This can be seen in figure 4.4, figure 4.5 and figure 4.6. Thus, we expect that by applying a higher grid resolution, the WGM pattern will appear for mode number 10 and higher. This shows clearly that the program I becomes more stable at a higher grid resolution.

Table 4.5: Wave function plots with corresponding mode number of the first five resonances from program I with grid resolution 50x50, 75x75 and 100x100 from figure 4.4, figure 4.5 and figure 4.6, respectively.

N	Grid res. 50x50	Grid res. 75x75	Grid res. 100x100
5	Program I: ν =606cm^{-1}	Program I: ν =604cm^{-1}	Program I: ν =603cm^{-1}
6	Program I: ν =710cm^{-1}	Program I: ν =707cm^{-1}	Program I: ν =704cm^{-1}
7	Program I: ν =812cm^{-1}	Program I: ν =808cm^{-1}	Program I: ν =801cm^{-1}
8	Program I: ν =913cm^{-1}	Program I: ν =909cm^{-1}	Program I: ν =904cm^{-1}
9	Program I: ν =1019cm^{-1}	Program I: ν =1008cm^{-1}	Program I: ν =1003cm^{-1}

The program and the simulations of grid resolution of 50x50 and 75x75 were done with success, while the simulations were initially, i.e. before the MATLAB program was vectorised, quite problematic for a grid resolution of 100x100. For each of the wavenumbers, the calculations took four hours at Stallo. Stallo has a limited walltime. Therefore, the interval containing 900 wavenumbers was divided into 20 wavenumbers intervals. The jobs with 20 wavenumbers were expected to give results after four days. A bug in the shell script made the jobs swap and used up the CPU hours given to the project at Stallo. Because of these obstacles and the limited time for a master thesis, a higher grid resolution then 100x100 could not be checked. Finally, the project was given more CPU hours and the remaining results were done with the modified vectorised program.

In figure 4.7, the integral of the squared absolute value of the wave function, $\left|\vec{\Psi}\right|^2$, over the area of the square framing the disk for the analytical solution (program III, figure 4.1) is compared to the integral of the squared absolute value of the wave function of the numerical solution (program I, figure 4.4). As grid resolution of 50x50 was used for program I. The wave function for the analytical program was plotted with a pixel resolution of 200x200. It is important to remember that the grid resolution defines the numerical accuracy of program I, while for program III, the pixel resolution only defines the resolution of the plot, since the solution is analytical. The wave function plots that correspond to the peaks of both graphs in figure 4.7 are plotted for comparison including their corresponding mode number in table 4.6. The difference between the wavenumber positions where the resonances appear for program I and program III, respectively are given as $\Delta\nu = \nu_I - \nu_{III}$, where ν_I is the wavenumber position of the respective peaks in the graph obtained by program I, while ν_{III} is the wavenumber position for the peaks in the graph obtaned by program III. As we can see from the table, the discrepancy $\Delta\nu$ increase as the wavenumber increases. Figure 4.8 and figure 4.9 show the same graphs as figure 4.7 but with grid resolution 75x75 and 100x100, respectively. For comparison, the graph of the numerical solution (program I) was scaled. Table 4.7 and table 4.8 show the same wave function plots as table 4.6, but for grid resolution 75x75 and 100x100, respectively.
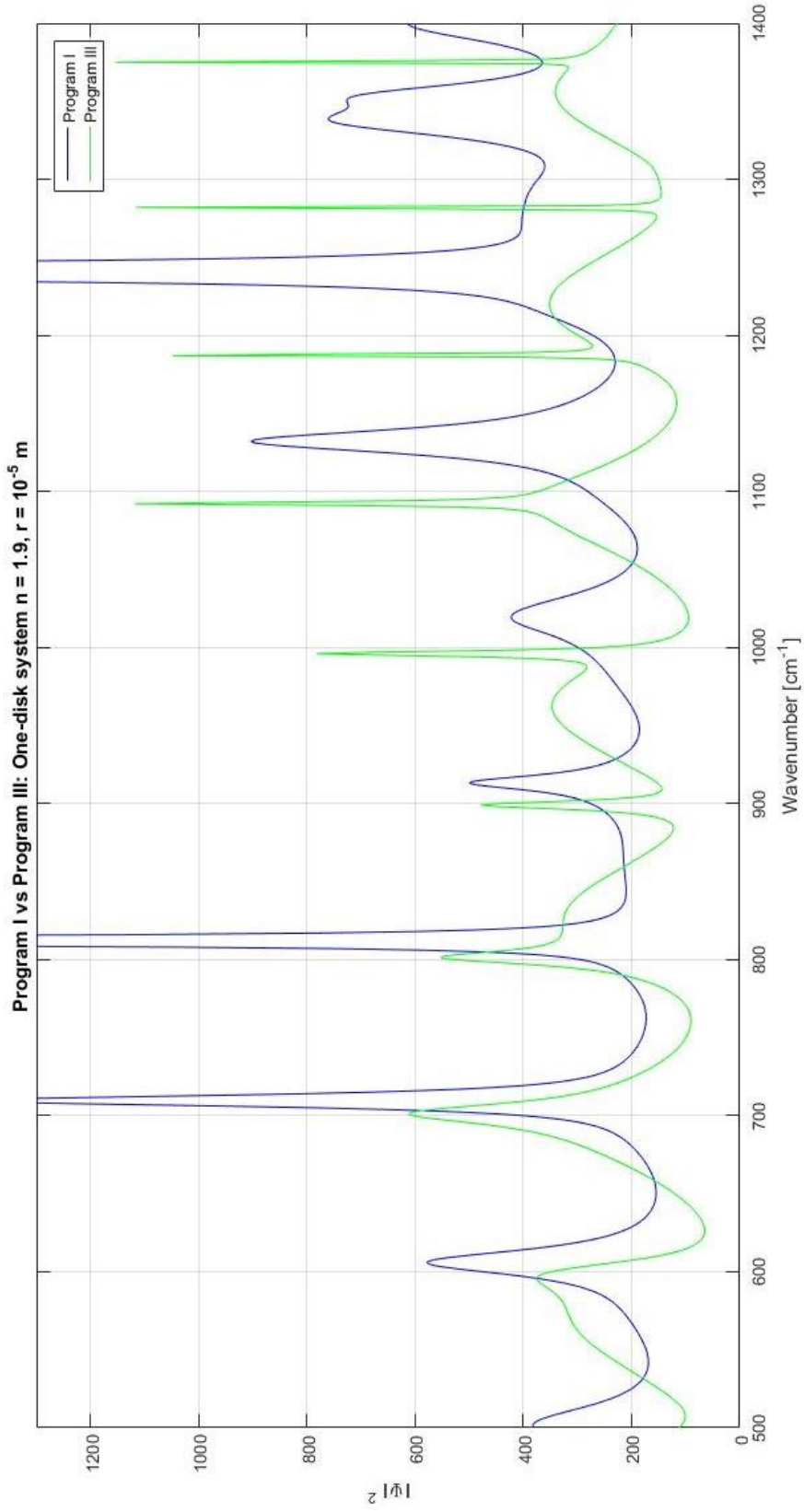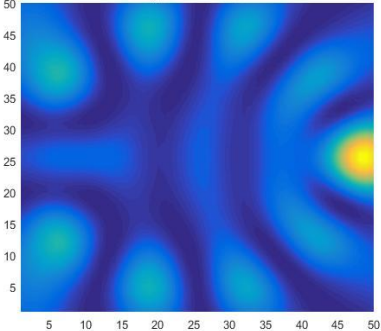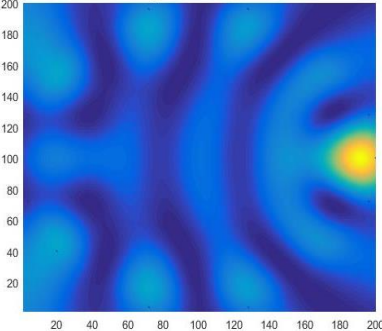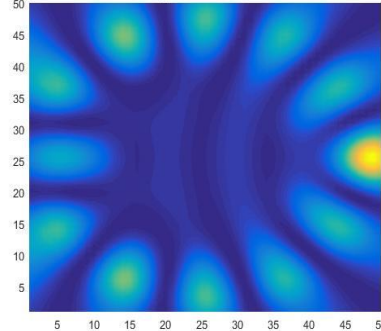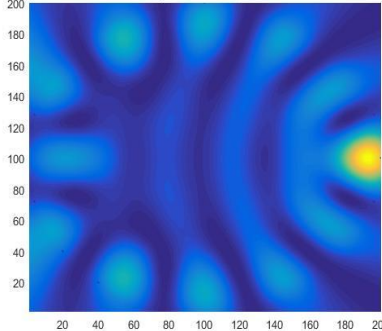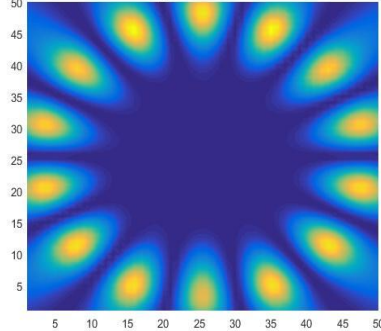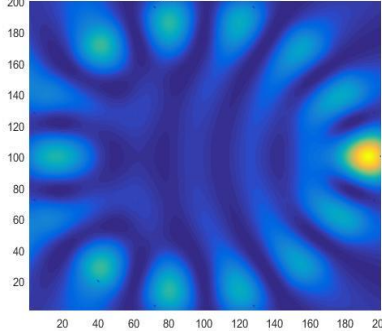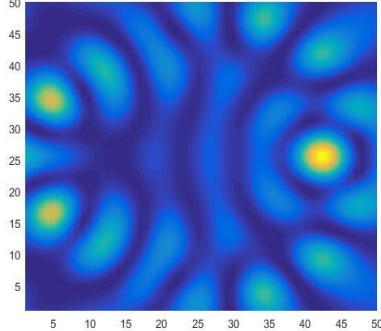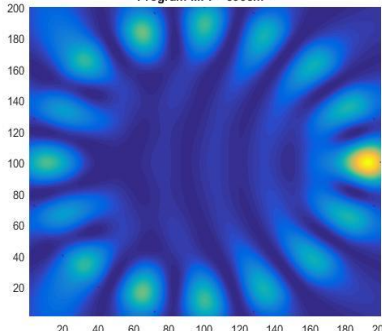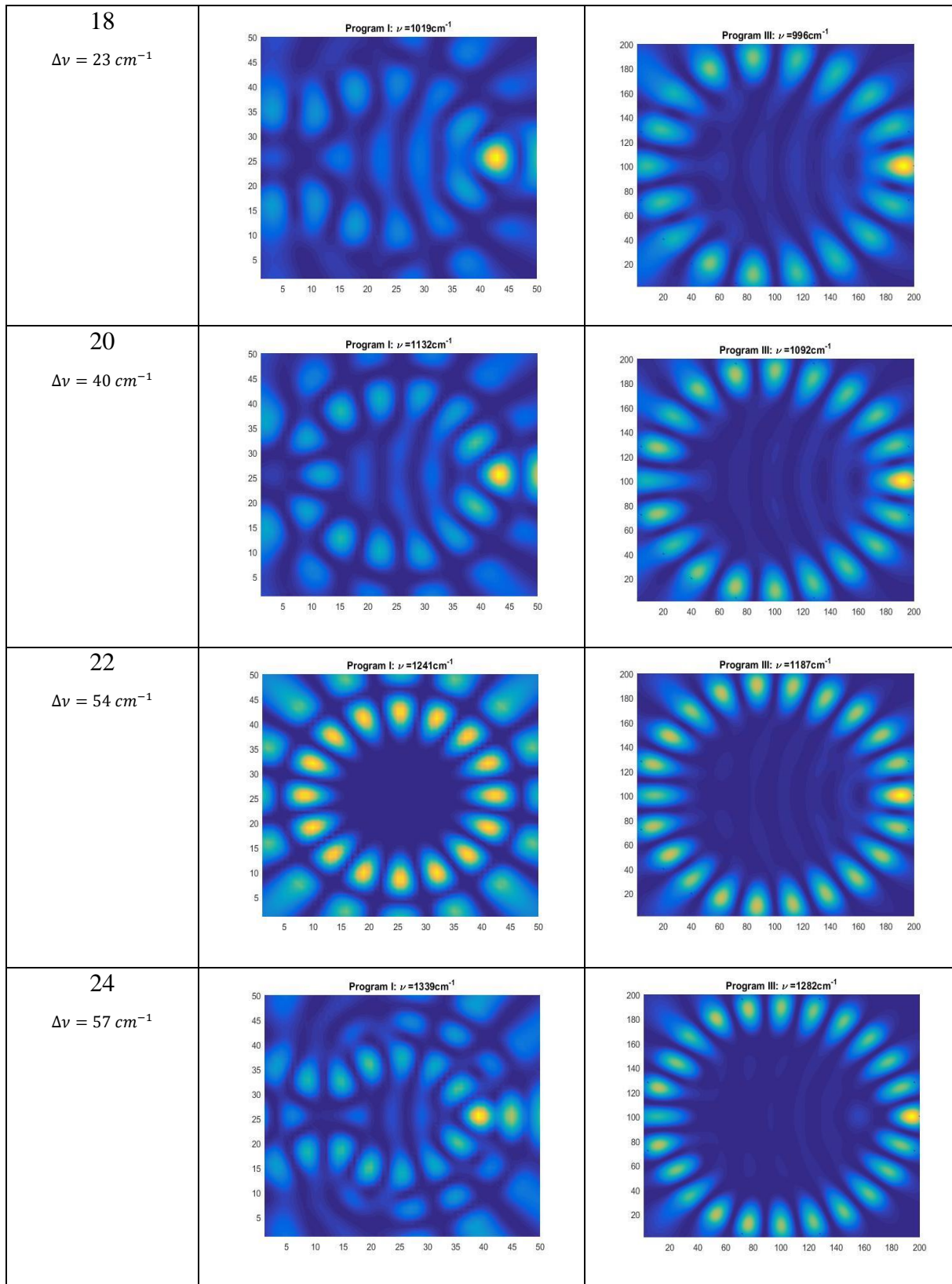
Figure 4.7: The blue line is the results from the analytical plane wave scatter solution (program III) in figure 4.1. The green line is the results from the numerical plane wave scatter solution (program I) for grid resolution 50x50 in figure 4.4. Both results is the integral of the squared absolute value of the wave function $|\Psi|^2$ plotted as a function of the wavenumber ν, for a plane wave coming from the left and impinging at a disk with 10 μm and a refractive index of 1.9.

Table 4.6: The wave function plots for the wavenumber positions of the resonances obtained by program I and III in figure 4.7 are shown in the columns in the middle and to the right, respectively. The mode number is displayed in the left column together with the discrepancy $\Delta\nu = \nu_I - \nu_{III}$ of the wavenumber positon at which the resonances appear for the two programs. For the numerical program (program I) a grid resolution of 50x50 was used.

Mode number $\Delta\nu = \nu_I - \nu_{III}$	Program I – Numerical plane wave scatter solution with grid 50x50	Program III – Analytical plane wave scatter solution
10 $\Delta\nu = 10\ cm^{-1}$		
12 $\Delta\nu = 9\ cm^{-1}$		
14 $\Delta\nu = 11\ cm^{-1}$		
16 $\Delta\nu = 14\ cm^{-1}$		

18 $\Delta \nu = 23\ cm^{-1}$	Program I: $\nu = 1019 cm^{-1}$	Program III: $\nu = 996 cm^{-1}$
20 $\Delta \nu = 40\ cm^{-1}$	Program I: $\nu = 1132 cm^{-1}$	Program III: $\nu = 1092 cm^{-1}$
22 $\Delta \nu = 54\ cm^{-1}$	Program I: $\nu = 1241 cm^{-1}$	Program III: $\nu = 1187 cm^{-1}$
24 $\Delta \nu = 57\ cm^{-1}$	Program I: $\nu = 1339 cm^{-1}$	Program III: $\nu = 1282 cm^{-1}$
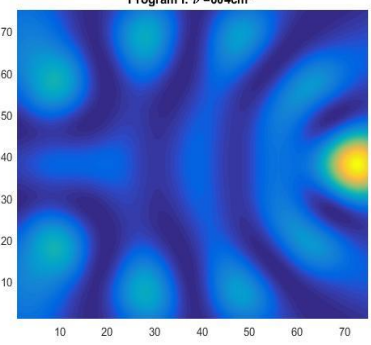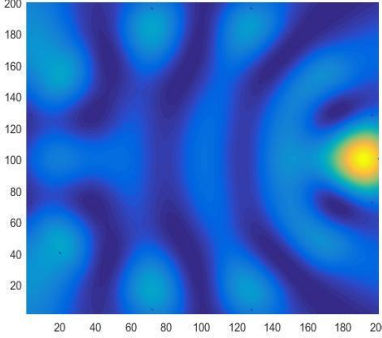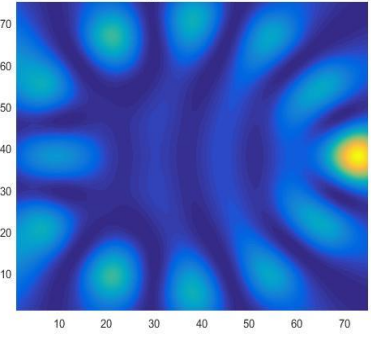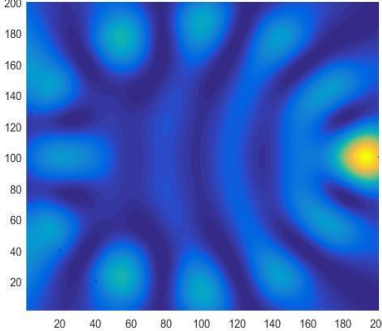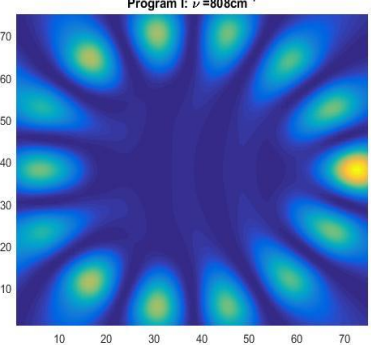
Figure 4.8: The blue line is the results from the analytical plane wave scatter solution (program III) in figure 4.1. The green line is the results from the numerical plane wave scatter solution (program I) for grid resolution 75x75 in figure 4.5. Both results is the integral of the squared absolute value of the wave function $|\Psi|^2$ plotted as a function of the wavenumber ν, for a plane wave coming from the left and impinging at a disk with 10 µm and a refractive index of 1.9.

41

Table 4.7: The wave function plots for the wavenumber positions of the resonances obtained by program I and III in figure 4.7 are shown in the columns in the middle and to the right, respectively. The mode number is displayed in the left column together with the discrepancy $\Delta\nu = \nu_I - \nu_{III}$ of the wavenumber positon at which the resonances appear for the two programs. For the numerical program (program I) a grid resolution of 75x75 was used.

Mode number $\Delta\nu = \nu_I - \nu_{III}$	Program I – Numerical plane wave scatter solution with grid 75x75	Program III - Analytical
5 $\Delta\nu = 8\ cm^{-1}$		
6 $\Delta\nu = 6\ cm^{-1}$		
7 $\Delta\nu = 7\ cm^{-1}$		
8 $\Delta\nu = 10\ cm^{-1}$		

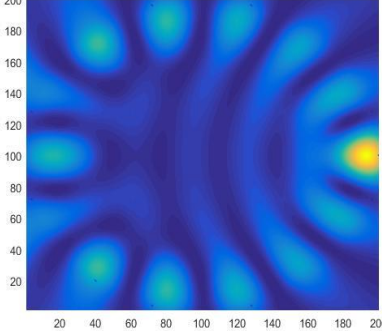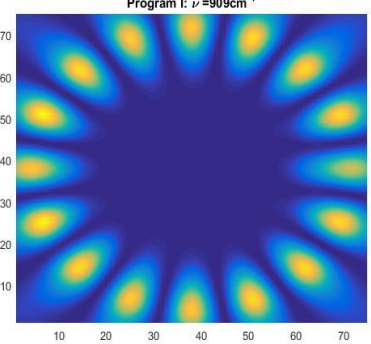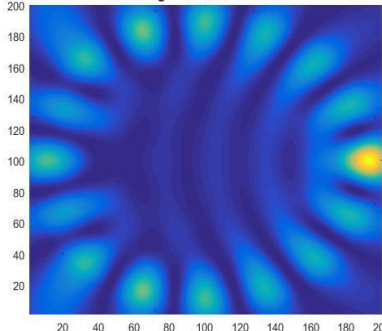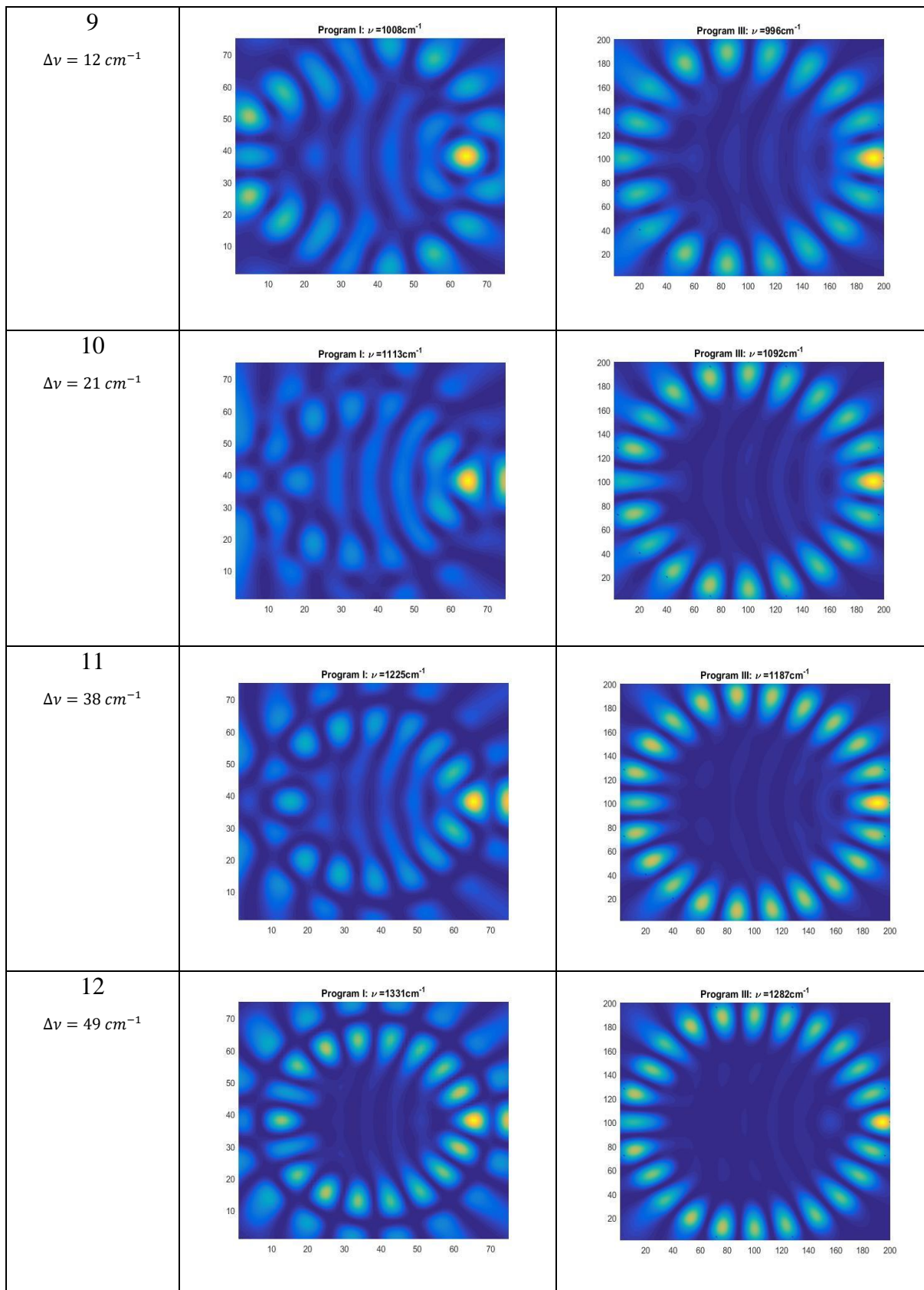| 9 $\Delta \nu = 12\ cm^{-1}$	Program I: $\nu =1008cm^{-1}$	Program III: $\nu =996cm^{-1}$
10 $\Delta \nu = 21\ cm^{-1}$	Program I: $\nu =1113cm^{-1}$	Program III: $\nu =1092cm^{-1}$
11 $\Delta \nu = 38\ cm^{-1}$	Program I: $\nu =1225cm^{-1}$	Program III: $\nu =1187cm^{-1}$
12 $\Delta \nu = 49\ cm^{-1}$	Program I: $\nu =1331cm^{-1}$	Program III: $\nu =1282cm^{-1}$
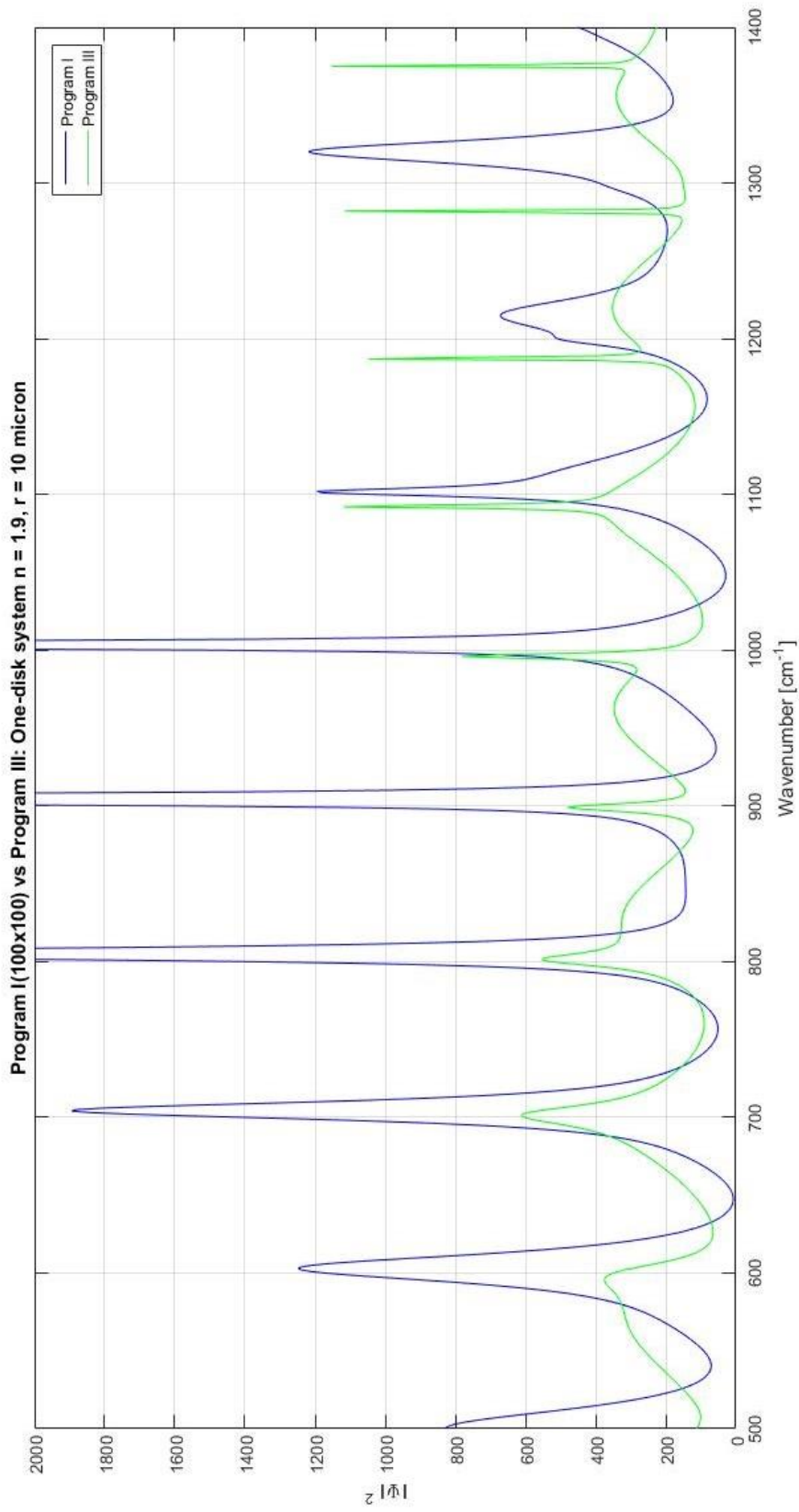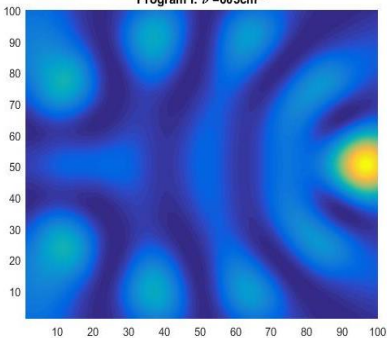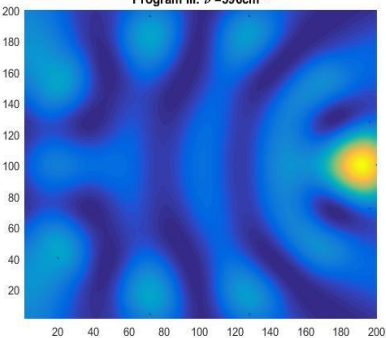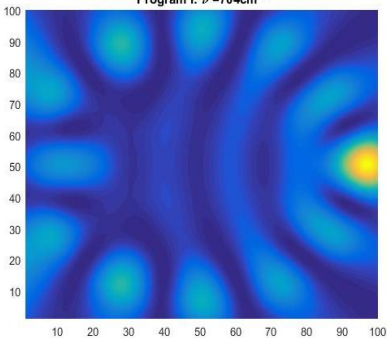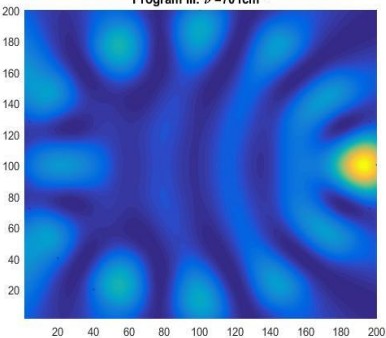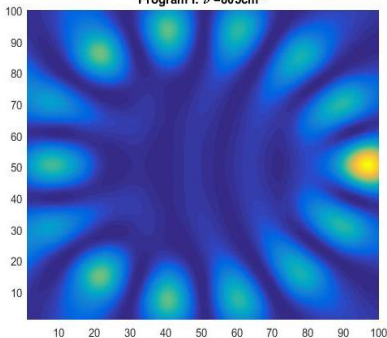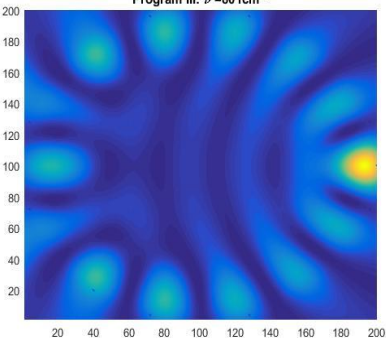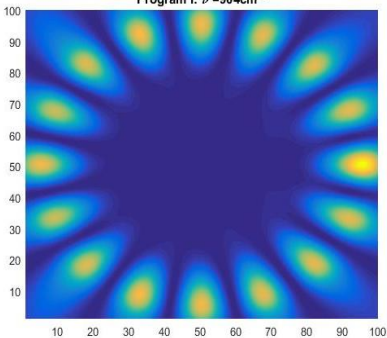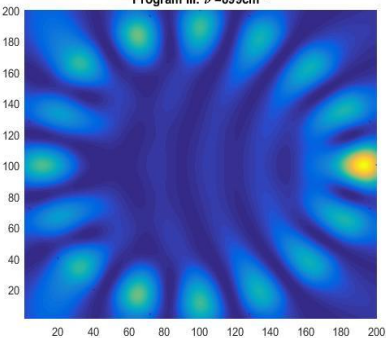
Figure 4.9: The blue line is the results from the analytical plane wave scatter solution (Program III) in figure 4.1. The green line is the results from the numerical plane wave scatter solution (program I) for grid resolution 100x100 in figure 4.5. Both results is the integral of the squared absolute value of the wave function $|\Psi|^2$ plotted as a function of the wavenumber v, for a plane wave coming from the left and impinging at a disk with 10 μm and a refractive index of 1.9.

Table 4.8: The wave function plots for the wavenumber positions of the resonances obtained by program I and III in figure 4.7 are shown in the columns in the middle and to the right, respectively. The mode number is displayed in the left column together with the discrepancy $\Delta \nu = \nu_I - \nu_{III}$ of the wavenumber positon at which the resonances appear for the two programs. For the numerical program (program I) a grid resolution of 100x100 was used.

Mode number $\Delta \nu = \nu_I - \nu_{III}$	Program I –Numerical plane wave scatter solution with grid 100x100	Program III - Analytical
5 $\Delta \nu = 7\ cm^{-1}$		
6 $\Delta \nu = 3\ cm^{-1}$		
7 $\Delta \nu = 4\ cm^{-1}$		
8 $\Delta \nu = 5\ cm^{-1}$		

9 $\Delta v = 7\ cm^{-1}$	Program I: $\nu = 1003 cm^{-1}$	Program III: $\nu = 996 cm^{-1}$
10 $\Delta v = 10\ cm^{-1}$	Program I: $\nu = 1102 cm^{-1}$	Program III: $\nu = 1092 cm^{-1}$
11 $\Delta v = 28\ cm^{-1}$	Program I: $\nu = 1215 cm^{-1}$	Program III: $\nu = 1187 cm^{-1}$
12 $\Delta v = 38\ cm^{-1}$	Program I: $\nu = 1320 cm^{-1}$	Program III: $\nu = 1282 cm^{-1}$

In table 4.9, the wavenumber positions for the resonances obtained by the numerical solution based on the Lippmann Schwinger (program I) are compared to the wavenumber positions of the resonances obtained by the analytical solutions (program III). In the first column, the Mode number of the respective resonance is given, the second column shows the wavenumber position obtained according to the analytical solution, while column 3-5 show the displacement of the respective resonance wavenumber obtained by program III for a grid resolution of 50x50, 75x75 and 100x100, respectively.

Table 4.9: The wave number position for the resonances obtained by the numerical solution based on the Lippmann Schwinger (program I) are compared to the wavenumber positions of the resonances obtain by the analytical solutions (program III). The first column the mode number to the respective resonances is given, the second column shows the wavenumber position obtained according to the analytical solution. Column 3-5 shows the displacement of the respective resonance wave numbers obtained by program III for a grid resolution of 50x50, 75x75 and 100x100, respectively.

Mode number	Program III wavenumber	Wavenumber displacement for program I (relative to wavenumbers from program III)		
		50x50	75x75	100x100
5	$596\ cm^{-1}$	$+\ 10\ cm^{-1}$	$+\ 8\ cm^{-1}$	$+\ 7\ cm^{-1}$
6	$701\ cm^{-1}$	$+\ 9\ cm^{-1}$	$+\ 6\ cm^{-1}$	$+\ 3\ cm^{-1}$
7	$801\ cm^{-1}$	$+\ 11\ cm^{-1}$	$+\ 7\ cm^{-1}$	$+\ 4\ cm^{-1}$
8	$899\ cm^{-1}$	$+\ 14\ cm^{-1}$	$+\ 10\ cm^{-1}$	$+\ 5\ cm^{-1}$
9	$996\ cm^{-1}$	$+\ 23\ cm^{-1}$	$+\ 12\ cm^{-1}$	$+\ 7\ cm^{-1}$
10	$1092\ cm^{-1}$	$+\ 40\ cm^{-1}$	$+\ 21\ cm^{-1}$	$+\ 10\ cm^{-1}$
11	$1187\ cm^{-1}$	$+\ 54\ cm^{-1}$	$+\ 38\ cm^{-1}$	$+\ 28\ cm^{-1}$
12	$1282\ cm^{-1}$	$+\ 57\ cm^{-1}$	$+\ 49\ cm^{-1}$	$+\ 38\ cm^{-1}$

As we can see in table 4.9, the displacement of the wavenumbers from program I decrease as the grid resolution increases. Hence, the grid resolution for 100x100 seems to be closer to the exact solution then the lower grid resolution. This indicates that if the grid resolution is further increased, the resonances move closer to the exact result. A visual inspection of the wave function plots in shows that for low wavenumber resonances (mode numbers 5,6 and 7), WGMs are revealed independently of the grid resolution used, while for high wavenumber resonances, a high resolution is required for revealing WGMs. This is due to the fact that for higher wavenumber resonances, the mode number and thus the number of nodes increases. With increasing mode number, the nodes become smaller and thus a higher grid resolution is needed. The size of each pixel depends on the grid resolution. Hence, for a grid resolution of

50x50 of a 10 micron radius disk, the pixel size is equal to $(0.4 \times 0.4)\mu m$, while for a grid resolution of 100x100 for the same disk the pixel size becomes $(0.2 \times 0.2)\mu m$. Since the area covered by one single node, decreases with increasing mode number, the pixel size need to decrease and the grid resolution needs to increase if one wants to achieve the same accuracy. This is obvious for the mode number 9 in table 4.5 where the grid resolution 50x50 and 75x75 resulted in a wavelength displacement for the resonances of $23 \ cm^{-1}$ and $12 \ cm^{-1}$, respectively (table 4.9) compared to the exact solution. For the grid resolution 100x100 though, the respective wave function plots (mode number 9 in table 4.5) shows the typical WGM pattern and the displacement was reduced to $7 \ cm^{-1}$ shown in table 4.9. In figures 4.7, 4.8, 4.9 and tables 4.6, 4.7, 4.8 we compared the wavenumber positions of resonances in the integral of the absolute value of the wave function over the square framing the disk. High discrepancies were found for resonance positions referring to high mode numbers and grid resolutions. In addition, wave function plots for the respective resonance positions were compared with each other. Another way to compare results is to consider the wavenumber positions for the resonances obtained by the analytical solution and plot the wave functions obtained by the numerical solution based on the Lippmann Schwinger equation for these exact wavenumber positions of the resonances. From the analytical scattering algorithm, program III, a Whispering gallery resonance with mode number $N = 7$ and 14 nodes at wavenumber $801 \ cm^{-1}$ was found (figure 4.1). The same resonance was found in program I at $812 \ cm^{-1}$, $808 \ cm^{-1}$ and $805 \ cm^{-1}$ with grid resolution 50x50, 75x75 and 100x100 (figure 4.4, figure 4.5, figure 4.6) respectably. We observed that the corresponding wave function plots deviated considerably for low grid resolutions. In order to study if the numerical program based on the Lippmann Schwinger equation can reveal WGMs at the exact resonance positions, program I was run with different grid resolutions (50x50, 70x70, 90x90, 110x110, 130x130 and 150x150) for the resonance wavenumber $801 \ cm^{-1}$. As seen table 4.10 in the resolution is stepwise changed from 50x50 to 150x150.

Table 4.10: Wave function plots for wavenumber $801 \; cm^{-1}$ *obtained by the numerical program based on the Lippmann Schwinger equation, program I, was run with six different grid resolutions, 50x50, 70x70, 90x90, 110x110, 130x130 and 150x150. The wavenumber position* $\nu = 801 \; cm^{-1}$ *with mode number N=7 and 14 nodes corresponds to a Whispering gallery resonance obtained by the analytical plane wave solution, program III.*

50x50	70x70
90x90	110x110
130x130	150x150
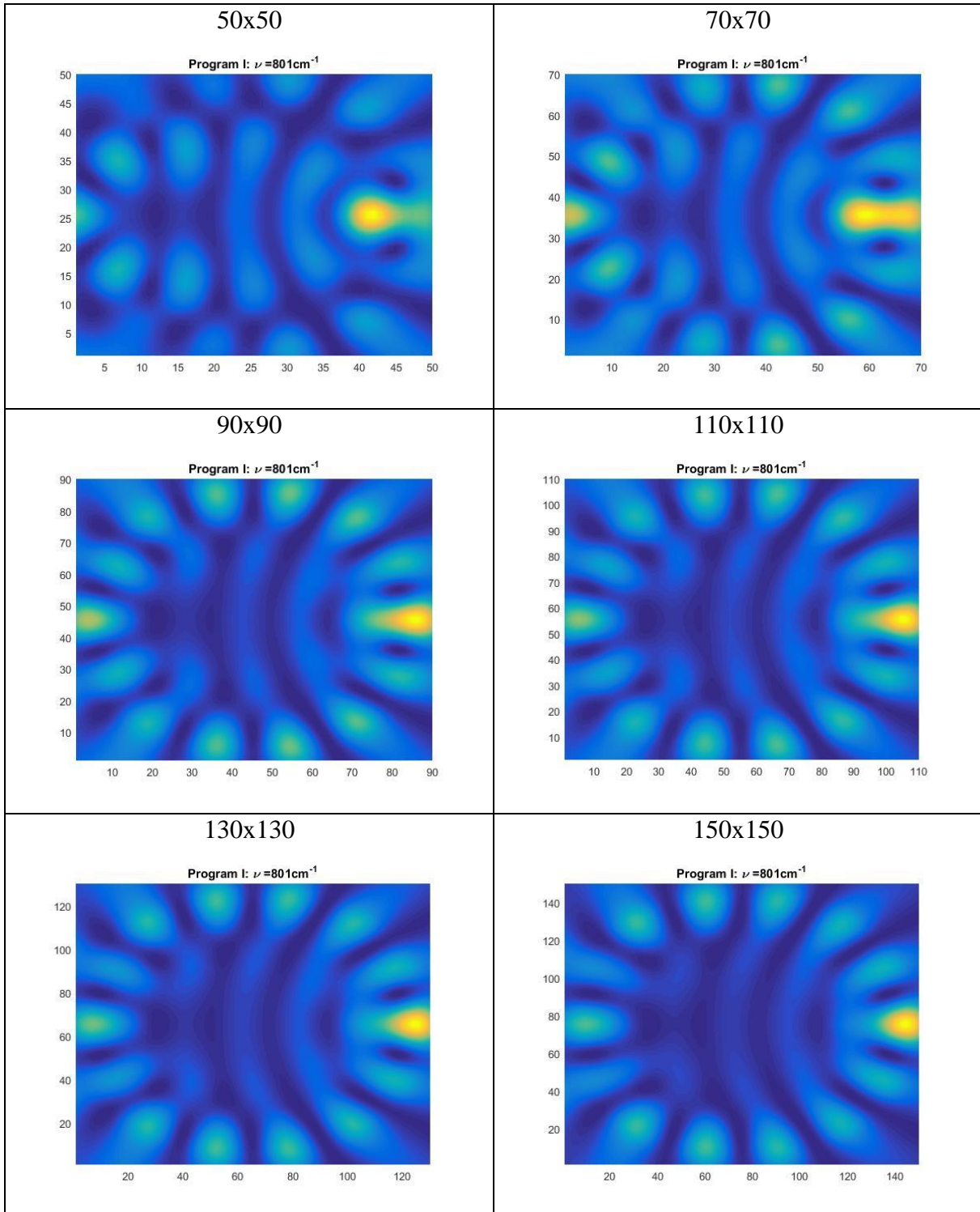
In table 4.10 we can observe that the wave inside the disk starts to form a Whispering gallery pattern as the grid resolution increases. For the grid resolution 90x90 and higher grid resolutions the typical WGM pattern can be observed.

The wave function plot obtained by program I with a grid resolution of 100x100 was autoscaled in MATLAB with color intensity scale 0-14, shown in figure 4.10.
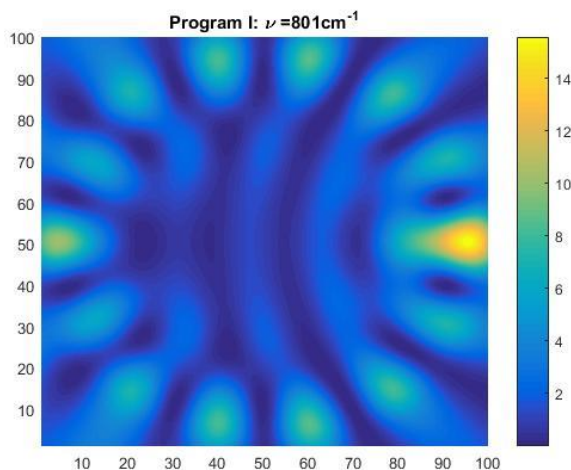
Figure 4.10: Wave function plot of $\nu = 801\ cm^{-1}$ obtained by program I with a grid resolution of 100x100. At right side of the plot, a colorbar with the range of intensity values 0 to 14 is displayed.

The wave function plot obtained by the analytical solution (program III) with a pixel resolution of 100x100 was autoscaled in MATLAB with color intensity scale 0-20, shown in figure 4.11b. In order to visually compare the wave function plot obtained by program I with a grid resolution of 100x100 in with the wave function plot obtained by program III with a grid solution of 100x100 the color intensity for the wave function plot for program I was rescaled from 0-14 to 0-20. Figure 4.11 shows the wave function plot (a) for program I and the wave function plot (b) for program III with the same colour scale of 0-20. In figure 4.11 we can see that the wave function plots displays the same type of pattern with 14 nodes inside the disk, while the absolute value of the brightest node to the right is slightly higher in the wave function obtained by program III. Comparing the wave function plot for program I with color scale 0-14 in figure 4.10 with wave function plot for program III with color scale 0-20 in figure 4.11b, the absolute value of the brightest node to the right appears to have the same brightness. As mentioned earlier the same resonance (mode number $N = 7$) found in program I with grid resolution 100x100 appeared at the wavenumber position $\nu = 805\ cm^{-1}$ (figure 4.6). If program I is run with a higher grid resolution then 100x100 the resonance with $N = 7$ may move to a wavenumber position of $\nu = 801\ cm^{-1}$, equal to the resonance wavenumber position of program III. Further investigation is necessary to analyse the color intensity scale

50

of the wave function plots of the resonances for program I with a higher grid resolution then done in this thesis.
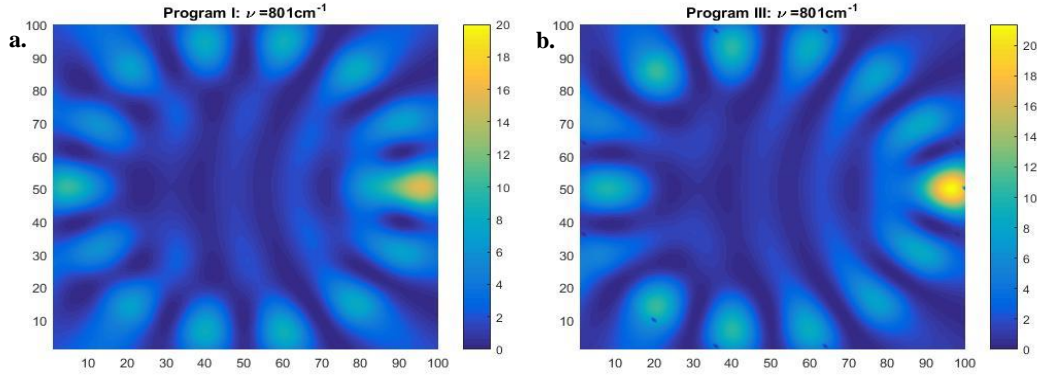
Figure 4.11: a) Wave function plot obtained by program I with a grid resolution of 100x100 and color scale intensity 0-20. b) Wave function plots obtained by program III with a pixel resolution of 100x100 and color scale intensity 0-20.

In order to estimate the error in the wave function plots obtained by program I which is based on the Lippmann Schwinger equation, we calculated the mean error of the absolute value of the wave function obtained by program I. This is done by subtracting in each pixel the squared absolute value of the wave function obtained by program I from the corresponding pixel value obtained by program III resulting in the discrepancy for each pixel. We calculate then for each pixel the absolute value of the discrepancy (error) and sum the error over all pixels. We divide this sum by the mean of the squared absolute value of the wave function obtained by the analytical solution (program III). The result we call relative pixel error. This is summarized in the two formula:

$$\Delta_{ij} = \sum_{i=1}^{100} \sum_{j=1}^{100} \frac{\left| \left| \Psi_{III\,i,j} \right|^2 - \left| \Psi_{I\,i,j} \right|^2 \right|}{mean} \tag{4.1}$$

where $\left| \Psi_{I\,i,j} \right|^2$ is squared absolute value of the wave function in element i,j obtained by program I and $\left| \Psi_{III\,i,j} \right|^2$ is squared absolute value of the wave function in element i,j obtained by program III and $mean = \frac{\sum_{i=1}^{100} \sum_{j=1}^{100} \left| \Psi_{III\,i,j} \right|^2}{Nx\,Ny}$. The relative pixel error is given by

$$\frac{\Delta_{ij}}{N_x\,N_y} \tag{4.2}$$

where N_x is number of pixels in *x*-direction and N_y is the number of pixels in *y*-direction. The relative pixel error is shown in figure 4.12 for different grid resolutions.
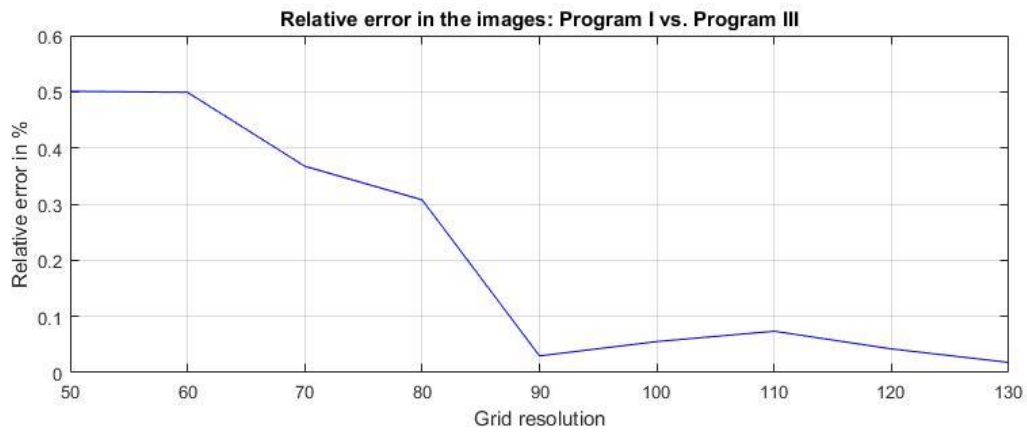
Figure 4.12: The relative pixel error gives in percent the difference in wave function plot from program I and the wave function plot for the wavenumber $\nu = 801\ cm^{-1}$ for different grid resolutions.

The relative pixel error troops from grid resolution 50x50 to 90x90. From grid resolution 90x90 to 130x130 the relative pixel error is quite stable around 0,5%. This indicates that the images for program I appearing from grid resolution 90x90 is relative alike the exact solution of the WGM pattern from Program III.

4.3 Program based on the analytical solution for the spherical wave scattering (program II)

In the following we evaluate the S-matrix for the scattering of a spherical wave at a disk (MATLAB script *SphericalWave_Scattering.m*, called program II) as described in section 3.3 is shown in Appendix C. From earlier results, we observed that the resonances from the numerical solution based on the Lippmann-Schwinger equation (program I) approaches the resonances from the analytical plane wave scattering solution (program III). Therefore, it made sense to compare the resonances of the S-matrix for the scattering of a spherical wave (program II) with the analytical solution for the scattering of a plane wave at a disk (program III). Program II was evaluated using a disk with a radius of $10 \ \mu m$ and a refractive index of 1.9. In figure 4.13a to figure 4.20a the real part of the denominator of the S-matrix is plotted in the region from $500 \ cm^{-1}$ to $1400 \ cm^{-1}$ for the orders $m = 0$ to $m = 9$. Resonances of the S-matrix are expected to appear when the real part of the denominator of the S-matrix is zero. For order number 0 to 7, the real part of the denominator of the S-matrix became zero twice. The corresponding wave functions at the zero-crossings are plotted in figure 4.13b,c-figure 4.18b,c. For order number 8 and 9 the real part of the denominator becomes zero once. The corresponding wave functions at the zero-crossings are plotted in figures 4.19b-4.20b. The wave functions are plotted by discretizing the disk into 200 grid cells in both x- and y-direction and calculating the intensity at every element $\left| \vec{\Psi}_j \right|^2$. All simulations were done on the author's computer.

The resonances are summarized in table 4.11 and compared with the resonances in the analytical plane wave scatter solution (program III). The resonance wavenumbers of the first zero crossings for order number 0 to 9 are marked with red text and placed at the nearest wavenumber from the analytical solution of the scattering of a plane wave at a disk (program III). The resonance wavenumber of the second zero crossings for order number 0 to7 are marked with blue text and compared to the nearest wavenumber from the plane wave scatter solution.

Table 4.11: The resonance wavenumbers from the analytical plane wave scattering resonances (program III) are displayed in the first column. The first row shows the resonance wavenumbers obtained by the spherical wave scattering solutions, i.e. where the denominator to the S-matrix is equal to zero. This is done for every order number separately. The red wavenumbers denote the first zero crossings, while the blue wavenumbers denote the second zero-crossings.

		Spherical wave																	
	Order no.	0		1		2		3		4		5		6		7		8	9
	Wave no. [cm^{-1}]	579	1116	507	1092	580	1116	672	1202	766	1157	861	1202	956	1292	1050	1387	1143	1236
Plane wave	596	579		507		580		672											
	701							672		766									
	801									766		861							
	899											861		965					
	996													956		1050			
	1092		1116		1092		1116				1157					1050		1143	
	1187		1116				1116		1202		1157		1202					1143	1236
	1282								1202				1202		1292				1236
	1375														1292		1387		

Table 4.11 shows that the resonances obtained by the zero-crossings of the real part of the S-matrix are not in accordance with the resonances obtained by the program based on the analytical solution of the plane wave scattering at the disk (program III). For program III, the resonances appears at nine different wavelengths while at for the spherical wave scatter solution (program II), the resonances appear once or twice depending on the order number. We can also observe that the resonance wavenumbers from program II appear at different numbers depending on the order number and resonance wavenumbers increase with increasing order.

Program II was checked to satisfy the properties i) and ii) from section 3.3. These properties hold. This indicates that the method was successfully implemented. Since the resonances obtained by the zero-crossings of the real part of the denominator of the S-matrix do not agree with the resonances obtained by the program based on the analytical solutions for the scattering of a plane wave at a disk, we assume that the imaginary part of the denominator also needs to be considered. This was unfortunately not possible in the frame of this thesis.

54

Zero order

denominator of S_0

a.

b. S_0:$nu_1 = 579 cm^{-1}$

c. S_0:$nu_2 = 1116 cm^{-1}$

Figure 4.13: a) The graph shows the real part of the denominator of the S-matrix for order number 0 as a function of the wavenumber.

b) Wave function plot of the first zero crossing of the denominator of the real part of the S-matrix in a).

c) Wave function plot of the second zero crossing of the denominator or the real part of the S-matrix in a).

First order

denominator of S_1

a.

b. S_1:$nu_1 = 507 cm^{-1}$

c. S_1:$nu_2 = 1092 cm^{-1}$

Figure 4.14: a) The graph shows the real part of the denominator of the S-matrix for order number 1 as a function of the wavenumber.

b) Wave function plot of the first zero crossing of the denominator of the real part of the S-matrix in a).

c) Wave function plot of the second zero crossing of the denominator or the real part of the S-matrix in a).

Second order

a.

denominator of S_2

Figure 4.15: a) The graph shows the real part of the denominator of the S-matrix for order number 2 as a function of the wavenumber.

b) Wave function plot of the first zero crossing of the denominator of the real part of the S-matrix in a).

c) Wave function plot of the second zero crossing of the denominator or the real part of the S-matrix in a).

b. $S_2:nu_1 = 580cm^{-1}$

c. $S_2:nu_2 = 1116cm^{-1}$
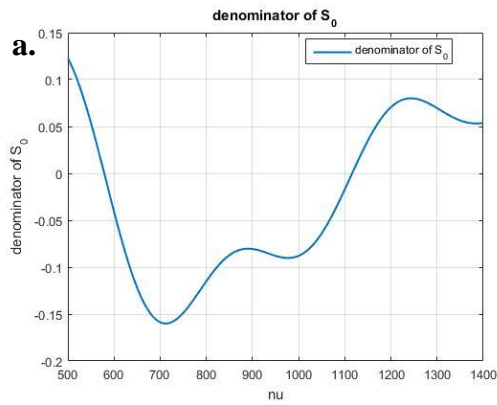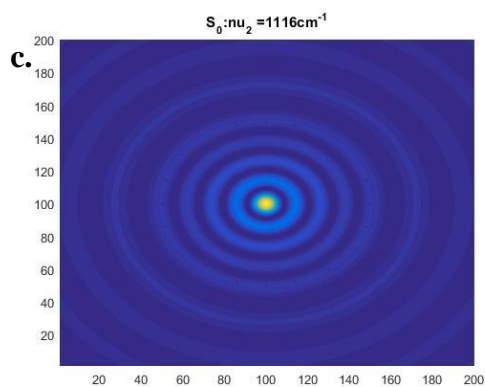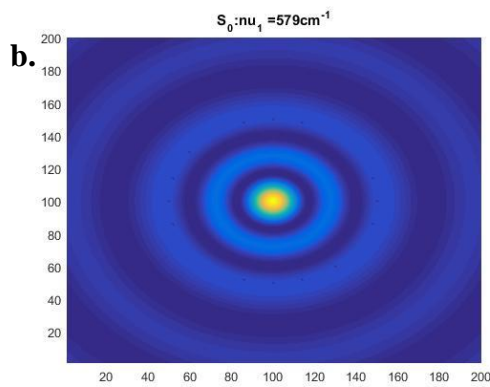
Third order

a.

denominator of S_3

Figure 4.16: a) The graph shows the real part of the denominator of the S-matrix for order number 3 as a function of the wavenumber.

b) Wave function plot of the first zero crossing of the denominator of the real part of the S-matrix in a).

c) Wave function plot of the second zero crossing of the denominator or the real part of the S-matrix in a).

b. $S_3:nu_1 = 672cm^{-1}$

c. $S_3:nu_2 = 1202cm^{-1}$

Fourth order

denominator of S₄

Figure 4.17: a) The graph shows the real part of the denominator of the S-matrix for order number 4 as a function of the wavenumber.

b) Wave function plot of the first zero crossing of the denominator of the real part of the S-matrix in a).

c) Wave function plot of the second zero crossing of the denominator or the real part of the S-matrix in a).

Fifth order
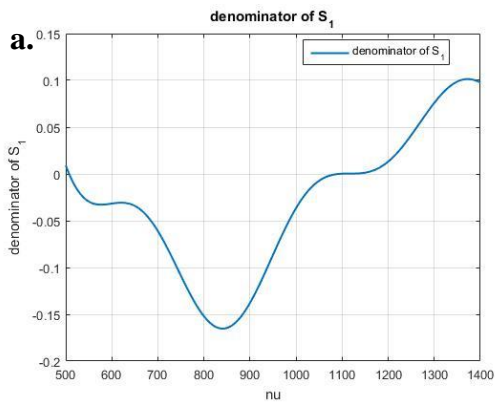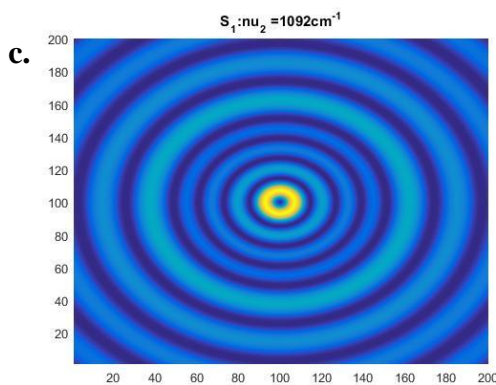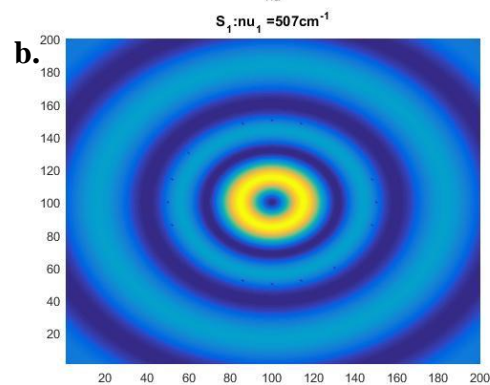

denominator of S₅

Figure 4.18: a) The graph shows the real part of the denominator of the S-matrix for order number 5 as a function of the wavenumber.

b) Wave function plot of the first zero crossing of the denominator of the real part of the S-matrix in a).

c) Wave function plot of the second zero crossing of the denominator or the real part of the S-matrix in a).

Sixth order

denominator of S_6

a.

b. $S_6 : nu_1 = 956 cm^{-1}$
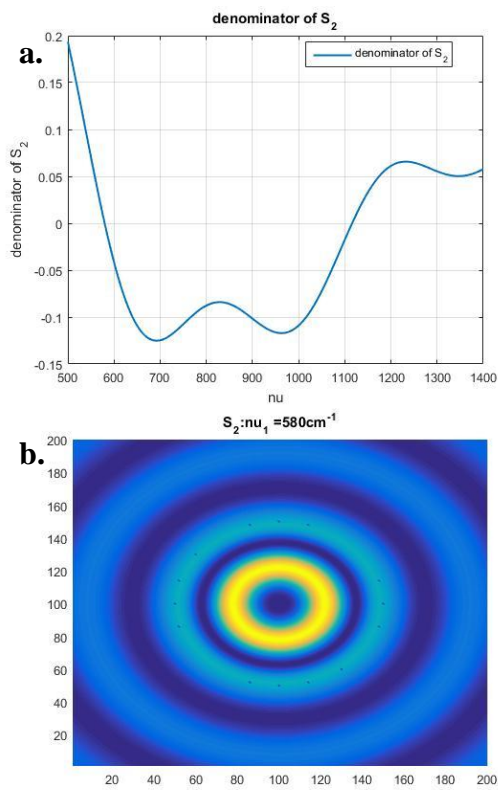
c. $S_6 : nu_2 = 1292 cm^{-1}$

Figure 4.19: a) The graph shows the real part of the denominator of the S-matrix for order number 6 as a function of the wavenumber.

b) Wave function plot of the first zero crossing of the denominator of the real part of the S-matrix in a).

c) Wave function plot of the second zero crossing of the denominator or the real part of the S-matrix in a).

Seventh order

denominator of S_7

a.

b. $S_7 : nu_1 = 1050 cm^{-1}$
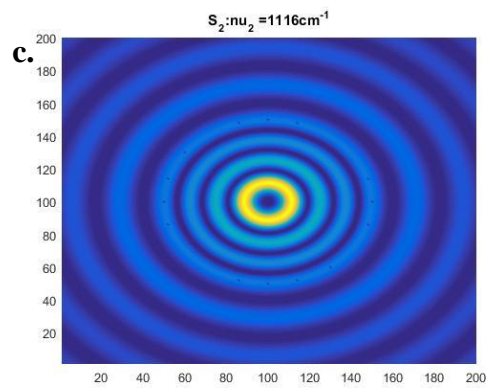
c. $S_7 : nu_2 = 1387 cm^{-1}$

Figure 4.20 a) The graph shows the real part of the denominator of the S-matrix for order number 7 as a function of the wavenumber.

b) Wave function plot of the first zero crossing of the denominator of the real part of the S-matrix in a).

c) Wave function plot of the second zero crossing of the denominator or the real part of the S-matrix in a).
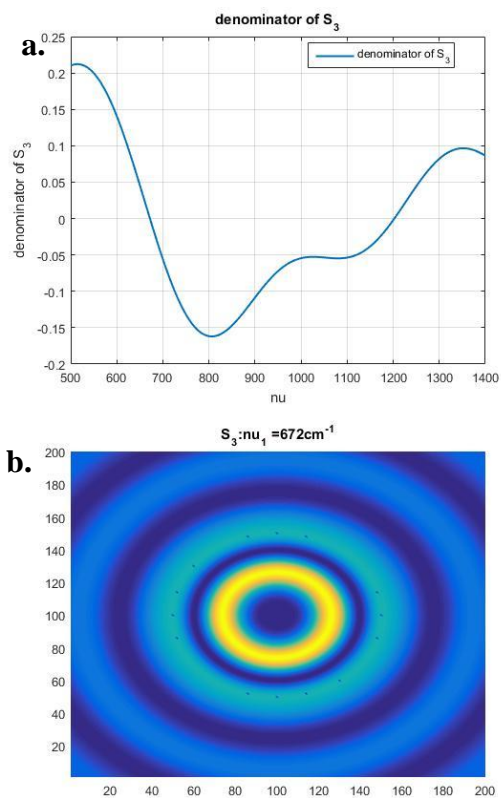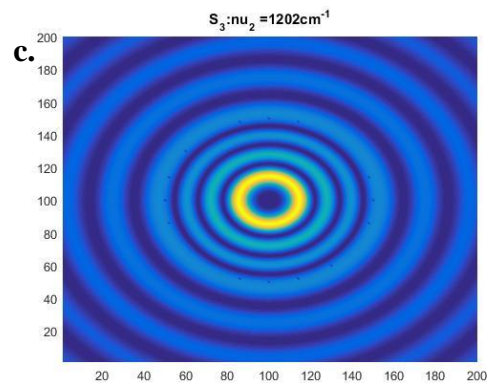
Eight order
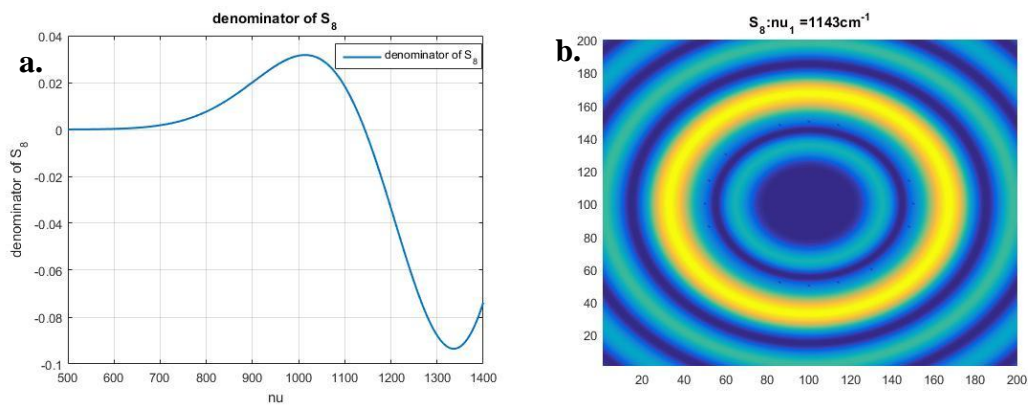
Figure 4.21: a) The graph shows the real part of the denominator of the S-matrix for order number 7 as a function of the wavenumber. b) Wave function plot of the first zero crossing of the denominator of the real part of the S-matrix in a).
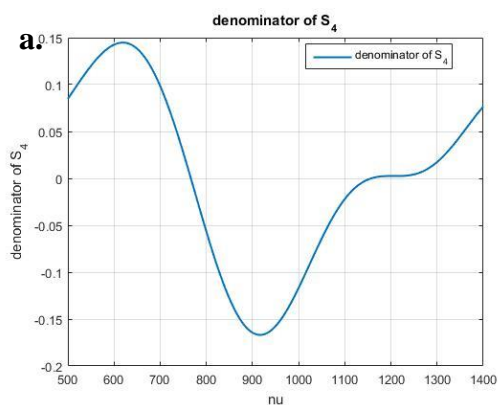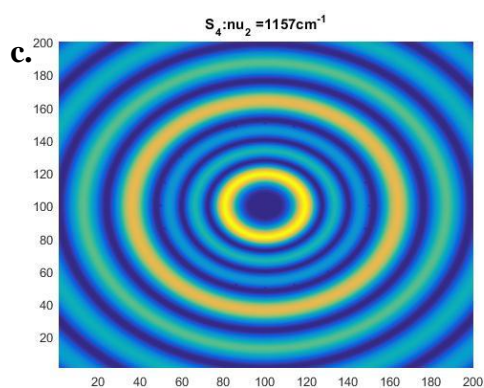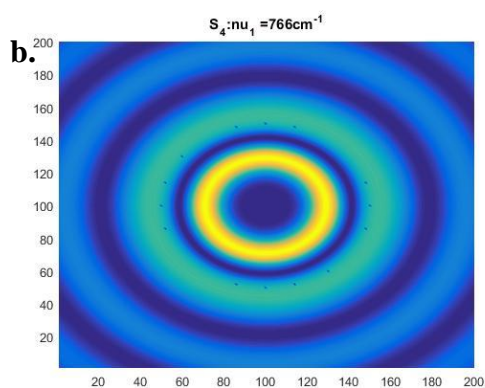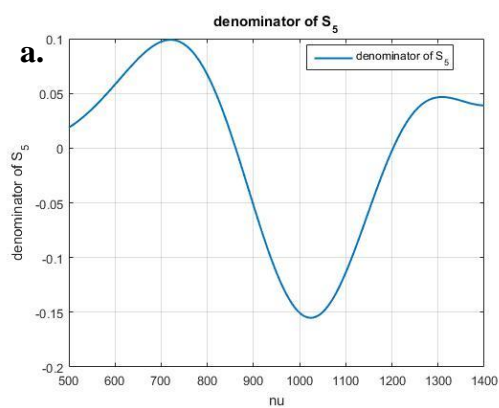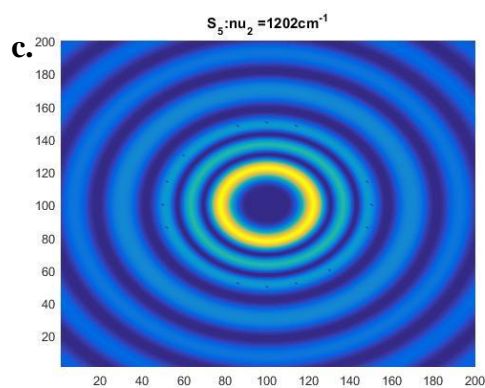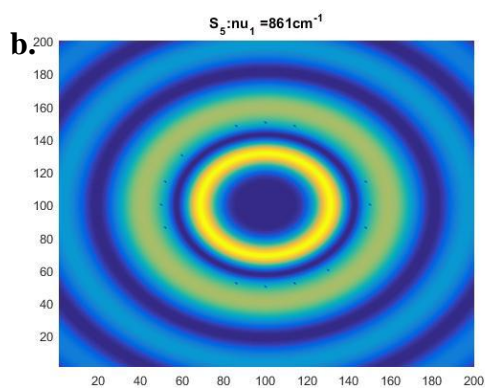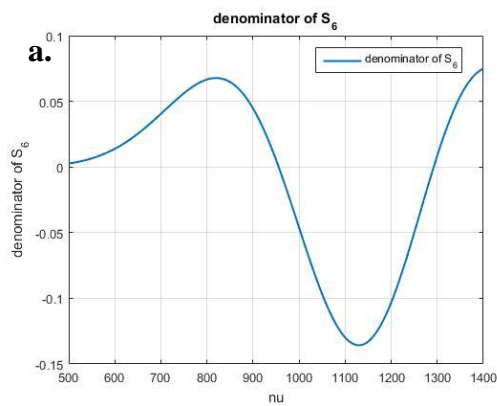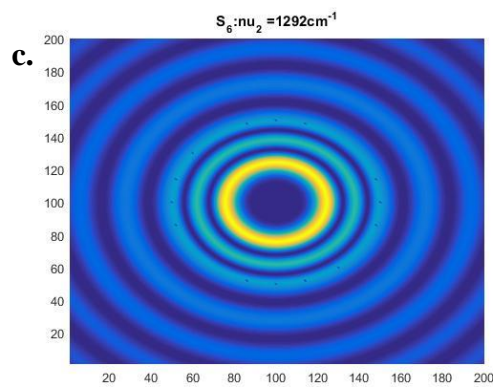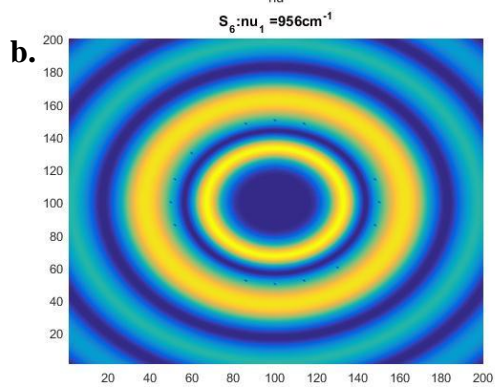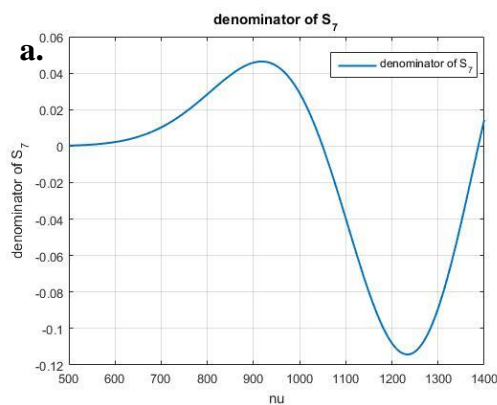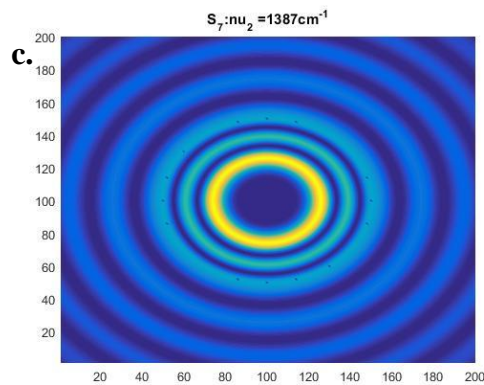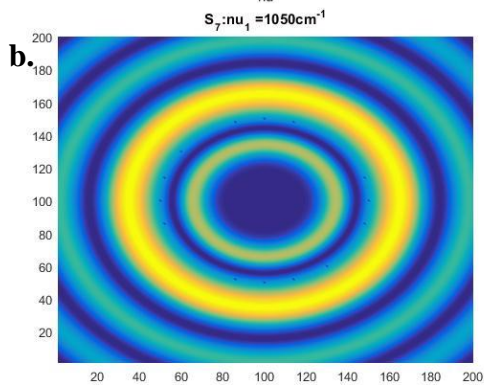
Ninth order
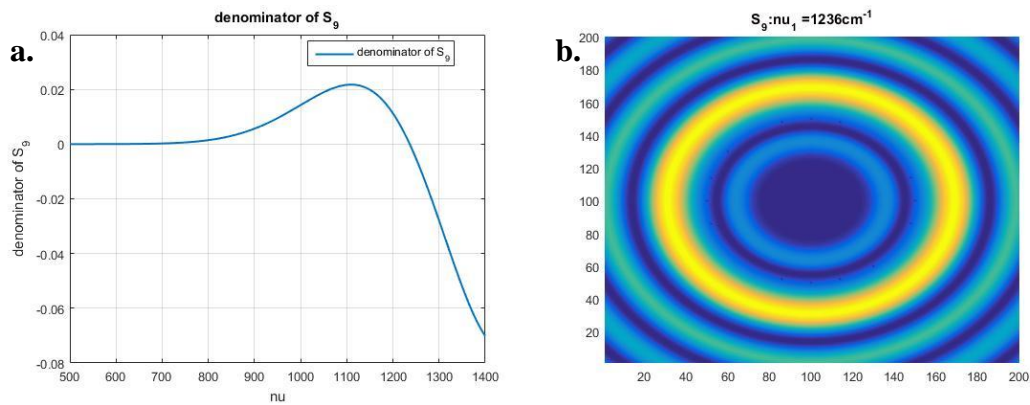
Figure 4.22: a) The graph shows the real part of the denominator of the S-matrix for order number 9 as a function of the wavenumber. b) Wave function plot of the first zero crossing of the denominator of the real part of the S-matrix in a).

4.4 Summary of the results and discussion

The results from section 4.1 shows that the analytical plane wave scatter algorithm was successfully implemented in MATLAB. The MATLAB program, called program III was referred to as the exact solution. Nine distinct resonances were observed in the wavenumber region from $500 \ cm^{-1}$ to $1400 \ cm^{-1}$ for a disk with a 10 micron radius and a refractive index of 1.9. These resonances could be explained by Whispering gallery modes. WGMs resonances are characterized by a pattern of bright nodes arranged in a regular order inside the disk. This characteristic pattern could be observed in the wave functions plots for the nine resonance wavenumbers. A quantization rule was set up relating the refractive index of the disk, the resonance wavelength, the mode number and the length of the ray trapped inside the disk, i.e. geometrical length. A comparison of the mode number calculated with the quantization rule using the geometrical length for polygonal whispering gallery ray and the circumference of an inscribed polygon in the disk showed a large degree of disagreement. Hence, the circumference of an inscribed polygon is not a good approximation for the geometrical length for a mode number up to $N = 13$. We further investigated if the pixel resolution effected the characteristics of the resonances in program I. The results showed that the pixel resolution did not influence the appearance of the resonances.

Section 4.2 shows the results from the numerical plane wave scatter algorithm (program I) for three different grid resolutions, 50x50, 75x75 and 100x100. Eight distinct resonances were observed in a disk with a 10 micron radius and refractive index of 1.9 in the wavenumber region from $500 \ cm^{-1}$ to $1400 \ cm^{-1}$. At the resonance wavenumbers, the wave function plots revealed the characteristic WGM patterns: in mode number 5,6 and 7 for grid resolution 50x50; in mode number 5,6,7 and 8 for grid resolution 75x75; and in mode number 5,6,7,8 and 9 for grid resolution 100x100. It is expected, that for a higher grid resolution the WGM pattern appears at higher mode numbers. This indicates that the increase of the grid resolution also increase the accuracy of program I.

The numerical results of program I based on the Lippmann Schwinger Equation were compared with the analytical solution for the scattering of a plane wave at a disk (program III). The results show that the resonances obtained by program I appear at higher wavenumbers than the corresponding resonances obtained by program III. As the grid resolution in program I increases, the discrepancy between the resonance positions for both programs decreases. As a result, the wavenumber positions of the resonances obtained by

program I become closer to the wavenumber positions of the resonances obtained by program III. We further notice that wave function plots with grid resolution 100x100 obtained by program III are in complete agreement with wave function plots obtained by program I for the first five resonances and all of them show the characteristic WGM pattern.

Further, we compared the wave function plots for mode number 7 at wavenumber $801 \; cm^{-1}$ obtained by program I and program III. The resonance wavenumber of mode number 7 shows discrepancy between the resonance positions of $11 \; cm^{-1}$ to $4 \; cm^{-1}$ for a grid resolution of 50x50 to 100x100, when comparing program I to program III. Nevertheless, already at 90x90 we can observe by visual inspection that the characteristic WGM pattern appears in the wave function plot obtained by program I. The increasing accuracy obtained when increasing the grid resolution is further confirmed by calculating the relative pixel error and plot this in a graph. From the graph we can see that the relative pixel error in the wave function plot is about 0.5% when the grid resolution is higher than 90x90.

The tests of the properties of the S-matrix in section 4.3 show that the analytical spherical wave scatter method was successfully implemented in MATLAB. The MATLAB program was called program II. The real part of the denominator of the S-matrix for a disk with 10 micron radius and refractive index of 1.9 was calculated and plotted against wavenumbers from $500 \; cm^{-1}$ to $1400 \; cm^{-1}$. This was done for orders 0 to 9. The S-matrix describes the intensity. When the denominator of the S-matrix is equal to zero, the intensity has a maximum. Hence, the zero crossing of the denominator is expected to correspond to resonances. For order number 0 to 7 two of these resonances appeared and for order number 8 and 9 one resonance appeared. These resonance wavenumbers were compared to the resonance wavenumbers obtained by program III. The comparison revealed no similarities. As both compared programs are analytical solutions, the resonance wavenumbers should agree for both programs. We assume that the discrepancy is due to the fact that only the real part of denominator of the S-matrix was considered in program II.

5 Conclusion and outlook

In this thesis, the focus was on the comparison of the numerical results of program I based on the Lippmann Schwinger Equation with the analytical solution for the scattering of a plane wave at a disk (program III). In addition, the S-matrix for the scattering of a spherical wave at a disk (program II) was considered and resonances of the S-matrix were compared with the program based on the Lippmann-Schwinger equation and the analytical solution for the scattering of a plane wave at a disk. The analytical plane wave scatter solution was successfully implemented as an algorithm (program III) and the results showed high stability. The results displayed distinct resonances in the disk that could be explained by Whispering gallery modes. We found a good agreement between the numerical solution (program I) and the analytical plane wave scattering solution (program III). First, we observed that the wavenumber positions of the resonances obtained by program III were systematically higher and that the discrepancy decreased with increasing grid resolution. We further observed that the discrepancy was larger for higher mode numbers. The wave function plots of the resonances for program I showed the appearance of Whispering gallery mode patterns in the first five of eight plots of the wavenumbers positions for resonances for a grid resolution of 100x100. For the two lower grid resolutions 50x50 and75x75, WGMs pattern appeared in 3 of 8 and 4 of 8 plots, respectively. These results indicated that the numerical program (program I) becomes more and more stable when the grid resolution increases. This shows that the wavenumber position for the resonances obtained by program I converges to the wavenumber positions for the resonances obtained by program III with increasing grid resolution and that the WGM pattern at higher wavenumber positions could also be revealed when the grid resolution is further increased. The simplification done for Green's function in program I, namely that the pole of the Green's function at zero was approximated by zero, seems to have little influence on the results. As further investigation, program I should be simulated with higher grid resolution then 100x100 for single disk, and check if the resonances appears at exactly the same position as the resonances in program III. A higher grid resolution should also be checked in program III with nanodisks and other refractive index. There are also other numerical methods suggested to solve scattering of a two-dimensional plane wave at multiple coupling disks. One is the finite difference time domain (FDTD) technique (Grandidier et al. 2011). The FDTD technique is very time consuming and requires extensive computation. It

would be interesting to compare the analytical results from program III with the FDTD technique and check the quality of this approach.

We compared the results from program II and program III and found no clear connection between the wavenumbers where the resonances appeared. The results from program II indicated that important information with respect to the resonances is lacking when only the real part of the denominator of the S-matrix was considered. Thus, both real and imaginary part of the denominator of the S-matrix needs to be considered.

Bibliography

Abramowitz, M. & Stegun, I. A. (1972). *Handbook of mathematical functions: with formulas, graphs, and mathematical tables*: Dover Publications, INC.

Brandsrud, M. A. (2015). *Understanding Resonant Structures of Coupled Disks for Light Management in Photovoltaics*. Master thesis. Ås: Norwegian University of Life Sciences Faculty of Environmental Science and Technology, Department of Mathematical Sciences and Technology. 78 pp.

Chen, C. J. (2011). *Physics of solar energy*: John Wiley & Sons.

Eisenlohr, J., Benick, J., Peters, M., Bläsi, B., Goldschmidt, J. C. & Hermle, M. (2014). Hexagonal sphere gratings for enhanced light trapping in crystalline silicon solar cells. *Optics Express*, 22 (S1): A111-A119.

Grandidier, J., Callahan, D. M., Munday, J. N. & Atwater, H. A. (2011). Light Absorption Enhancement in Thin-Film Solar Cells Using Whispering Gallery Modes in Dielectric Nanospheres. *Advanced Materials*, 23 (10): 1272-1276.

Grandidier, J., Weitekamp, R. A., Deceglie, M. G., Callahan, D. M., Battaglia, C., Bukowsky, C. R., Ballif, C., Grubbs, R. H. & Atwater, H. A. (2013). Solar cell efficiency enhancement via light trapping in printable resonant dielectric nanosphere arrays. *physica status solidi (a)*, 210 (2): 255-260.

Green, G. (1828). *An essay on the application of mathematical analysis to the theories of electricity and magnetism*: Author.

Kirsch, A. & Hettlich, F. (2009). The Mathematical Theory of Maxwell's Equations. *Lecture notes*.

Kokhanovsky, A. A. (2011). *Light Scattering Reviews, Vol. 6*. Light scattering reviews. Dordrecht: Springer.

Oraevsky, A. N. (2002). Whispering-gallery waves. *Quantum Electronics*, 32 (5): 377-400.

Pachauri, R. K., Allen, M., Barros, V., Broome, J., Cramer, W., Christ, R., Church, J., Clarke, L., Dahe, Q. & Dasgupta, P. (2014). Climate Change 2014: Synthesis Report. Contribution of Working Groups I, II and III to the Fifth Assessment Report of the Intergovernmental Panel on Climate Change.

Sharma, S. K. & Sommerford, D. J. (2006). *Light scattering by optically soft particles: theory and applications*: Springer Science & Business Media.

Tipler, P. A. & Mosca, G. (2004). *Physics for scientists and engineers*. 5th ed., Standard version. ed. New York: Freeman.

Townsend, J. S. (2010). *Quantum Physics: A Fundamental Approach to Modern Physics*: University Science Books.

Wallentin, J., Anttu, N., Asoli, D., Huffman, M., Åberg, I., Magnusson, M. H., Siefer, G., Fuss-Kailuweit, P., Dimroth, F., Witzigmann, B., et al. (2013). InP Nanowire Array Solar Cells Achieving 13.8% Efficiency by Exceeding the Ray Optics Limit. *Science*, 339 (6123): 1057-1060.

Zhu, J., Hsu, C.-M., Yu, Z., Fan, S. & Cui, Y. (2009). Nanodome solar cells with efficient light management and self-cleaning. *Nano letters*, 10 (6): 1979-1984.

Appendix A

The MATLAB scripts for program III is enclosed in Appendix A:

- *ProgramIII.m*

    The analytical plane wave method is implemented as an algorithm in this script.

    Calculates the squared absolute value of the wave function for series of wavenumbers.

    When the input is only one wavenumber a plotted image is displayed.

- *constant_planewave.m*

    A function that gives the parameters A_l and B_l.

```matlab
%%%%%%%%%%%%%%%%%%%%%%%%%%%%%%%%%%%%%%%%%%%%%%%%%%%%%%%%%%%%%%%%%%%%%%%%%%%
%     ProgramIII.m                                                       %
%                                                                        %
%     Frida H.M Torgersen                                                %
%                                                                        %
%     Program III based on the analytical plane wave scattering method   %
%                                                                        %
%%%%%%%%%%%%%%%%%%%%%%%%%%%%%%%%%%%%%%%%%%%%%%%%%%%%%%%%%%%%%%%%%%%%%%%%%%%


clear all
close all


%% _____ properties that can be changed_____
%_____disk_____

n = 1.9; % Refractive index
a = power(10,-5); % Radius


l = -20:1:20;    % Interval of order
h = length(l);

%%_____ Light_____

nu = 801; % Wavenumber
kArr = nu*100*2*pi; % angular wavenumber outside the disk


betaArr = kArr*n; % angular wavenumber inside the disk




%% Grid
```

```matlab
Sum_psiArr = zeros(1,length(nu));
    aa=1; %Change the frame, aa=1 the frame goes around the disk
    X0=-aa*a;
    Y0=-aa*a;
    Nstep=200; % Grid size
    step=2*aa*a/Nstep;

for jnu = 1:length(nu);

    Psii = zeros(Nstep,Nstep);
    Psi=zeros(Nstep,Nstep);
    absPsii = zeros(Nstep,Nstep);

    k = kArr(jnu);
    beta = betaArr(jnu);
    [A_l,B_l]= constants_planewave(l,a,k,beta,n);


    for i=1:Nstep
        x=X0+step*double(i);
        for j=1:Nstep
            y=Y0+step*double(j);
            theta1=atan2(y,x);
            r1=sqrt(x*x+y*y);
            for jk = 1:length(l)
                if (r1<a)
                    psi=besselj(l(jk),beta*r1)*exp(1i*l(jk)*theta1);
                    Psi(j,i)= B_l(jk)*psi;
                    Psii(j,i) = Psii(j,i)+ Psi(j,i);
                elseif (r1>a)
                    h1=(1i^l(jk))*besselj(l(jk),k*r1)*exp(1i*l(jk)*theta1);
                    h2=A_l(jk)*besselh(l(jk),1,k*r1)*exp(1i*l(jk)*theta1);
                    Psi(j,i)=h1+h2;
                    Psii(j,i) = Psii(j,i)+ Psi(j,i);
                end

            end
            absPsii(j,i) = abs(Psii(j,i)).*abs(Psii(j,i));
        end

    end




B(jnu,:) = sum(absPsii);
A(jnu) = sum(B(jnu));

if length(nu) > 1

    filename =
strcat('program3_n1.9_',num2str(nu(1)),'_',num2str(nu(end)),'_10micron.txt'
);

    g=fopen(filename,'a');

    fprintf(g,'%f    ',nu(jnu));

    fprintf(g,'%f\n', A(jnu));

ii
```

```matlab
        fclose(g);

    else
    filename=['Psii_peak_n1.9_',num2str(nu),'.mat'];

        save(filename);
    end
end

%___ Plotting the figure____

nu = k./(2*pi*100);
ZAbsWaveFunction.d=abs(Psii).*abs(Psii);

if(1)
    figure;
    set(gcf,'Color',[1 1 1]);
    pcolor(ZAbsWaveFunction.d);
    shading interp;
    colorbar;
    string = strcat('Program III: \nu =',int2str(nu),'cm^-1');
    title(string);
end
```

```matlab
%%%%%%%%%%%%%%%%%%%%%%%%%%%%%%%%%%%%%%%%%%%%%%%%%%%%%%%%%%%%%%%%%%%%%%%%%%%%%
%     constants_planewave.m                                               %
%                                                                         %
%     Frida H.M Torgersen                                                 %
%                                                                         %
%     A function that gives two constants A_l and B_l.                    %
%%%%%%%%%%%%%%%%%%%%%%%%%%%%%%%%%%%%%%%%%%%%%%%%%%%%%%%%%%%%%%%%%%%%%%%%%%%%%


function [A_l,B_l] = constants_planewave(l,a,k,beta,n)

for i= 1:length(l)
    for j = 1:length(k)
        Jk = besselj(l(i),k(j)*a);
        JK = besselj(l(i),beta(j)*a);
        if l(i) == 0
            dJk = -besselj(1,k(j)*a);      %dJ_0 = -J_1
            dJK = -n*besselj(1,beta(j)*a);
        else
            dJk = 0.5*(besselj(l(i)-1,k(j)*a)-besselj(l(i)+1,k(j)*a));
            dJK = 0.5*n*(besselj(l(i)-1,beta(j)*a)-
besselj(l(i)+1,beta(j)*a));
        end

        H1 = besselh(l(i),1,k(j)*a);
        if l(i) == 0
            dH1 = -besselh(1,1,k(j)*a); % dH1_0 = -H1_1
        else
            dH1 = 0.5*(besselh(l(i)-1,1,k(j)*a)-besselh(l(i)+1,1,k(j)*a));
        end


        NominatorA_l(i,j) = (1i^l(i))*(dJk*JK-Jk*dJK);
        DenominatorA_l(i,j) = H1*dJK-dH1*JK;

        A_l(i,j) = NominatorA_l(i,j)./DenominatorA_l(i,j);

        NominatorB_l(i,j) = (1i^l(i))*(dH1*Jk-dJk*H1);
        DenominatorB_l(i,j) = JK*dH1 -dJK*H1;

        B_l(i,j) = NominatorB_l(i,j)./DenominatorB_l(i,j);



    end
end

end
```

Appendix B

The MATLAB scripts for program I is enclosed in Appendix B:

- *Disk_Scattering20082015vec.m*

    The numerical plane wave method is implemented as an algorithm in this script.

    Calculates the squared absolute value of the wave function for series of wavenumbers.

    When the input is only one wavenumber a image is displayed.

```matlab
%%%%%%%%%%%%%%%%%%%%%%%%%%%%%%%%%%%%%%%%%%%%%%%%%%%%%%%%%%%%%%%%%%%%%%%%%%%%
%     Disk_Scattering20082015vec.m                                       %
%                                                                        %
%     Achim Kohler                                                       %
%     Modified by: Rozalia Lukacs                                        %
%                                                                        %
%     Program I based on the numerical plane wave scattering solution    %
%%%%%%%%%%%%%%%%%%%%%%%%%%%%%%%%%%%%%%%%%%%%%%%%%%%%%%%%%%%%%%%%%%%%%%%%%%%%


%_____Light_____%
% Chose the first nu_array if you want a series of wavenumbers, the second
% nu_array if you want for one wave number. Remember to comment out the one
% you do not use.

nu_array = [500 1400];    % Series of wavenumbers
% nu_array = (596);          % One wavenumber

NX=50;      %Grid resolution
NY=NX;


for nu= nu_array(1):1:nu_array(end)

    close all;

    ArrayOfCircles=1;
    Zebra=0;



    nu= nu * 100.0; % at 1000cm^(-1)

    phi = pi;    % angle of incident plane wave. For phi=0, the plane wave
    %is coming from the right. phi=pi/2, the plane wave is coming from the
    %top. phi = pi, plane wave coming from the left and so on..

    k=2*pi*nu;
    kx=k*cos(phi);
    ky=k*sin(phi);
    clear phi;

    NCx=1;
    NCy=1;
```

```matlab
    R= power(10,-5);   % Radius of the disk
    Nx=NX;
    Ny=NY;
    N=Nx*Ny;
    a=2*NCx*R;
    b=2*NCy*R;
    n_index=1.9;

    dx=a/Nx; % spacing in x-direction
    dy=b/Ny; % spacing in y-direction

    x0=0;
    y0=0;
    % x0=0.1*R;          % Can be used if you want to increase the frame
    % y0=0.1*R;
    Nxadd = (2*x0)./dx;
    Nyadd = (2*y0)./dy;
    Nx = Nx + Nxadd;
    Ny = Ny + Nyadd;
    N = Nx*Ny;

    x=zeros(1,N);
    y=zeros(1,N);

    indexi=reshape(((1:1:Nx)'*ones(1,Ny))',1,N);
    indexl=reshape(((1:1:Nx)'*ones(1,Ny)),1,N);

    indexj=(indexl-1).*Nx+indexi;
    x(indexj)=((indexi-0.5).*dx); % the Descartes coordiante x
    y(indexj)=((indexl-0.5).*dy); % the Descartes coordinate y

    jj = reshape(((1:1:N)'*ones(1,N))',1,N*N);
    mm = reshape(((1:1:N)'*ones(1,N)),1,N*N);

    Z = k*sqrt((x(jj)-x(mm)).*(x(jj)-x(mm))+(y(jj)-y(mm)).*(y(jj)-y(mm)));
    G = reshape(besselh(0,Z),N,N);
    G(isnan(G)) = 0 ;

    % Establish the potential

    v=zeros(1,N,'double');

    for m=1:N
        for nx=1:NCx
            for ny=1:NCy

                if (ArrayOfCircles)
                    % Array of circles
                    xcircle=(2*nx-1)*R+x0;
                    ycircle=(2*ny-1)*R+y0;

                    rn=sqrt((x(m)-xcircle)*(x(m)-xcircle)+(y(m)-
ycircle)*(y(m)-ycircle));
                    if (rn<R)
                        v(m)=1.0-n_index*n_index;
                    end
                end

            end
```

vi

```matlab
        end

    end

    Gtilde(1:N,:)=G(1:N,:).*reshape(reshape((v'*ones(1,N))',1,N*N),N,N);

    clear G;
    clear v;

    eikr=exp(1i*(kx*x+ky*y));

    clear x y;

    IdentityMat=eye(N,N);
    M=IdentityMat+1i*(k*k*dx*dy*0.25)*Gtilde;

    clear Gtilde;
    clear IdentityMat;



    %% Solve Linear Equation by Matlab routine

    psi_complex = linsolve(M,eikr');
    psi_complex_reshaped=reshape(psi_complex,Nx,Ny);

    Xplot=abs(psi_complex_reshaped).*abs(psi_complex_reshaped);

    linearIndexXplot=sub2ind(size(Xplot),Nx,Ny);
    IntegralPsi=sum(Xplot(1:linearIndexXplot));

%%____Display a image____%%
% When calculating one wavenumber an image can be displayed if the
% following is uncommented

%      figure;
%      pcolor(Xplot');
%      set(gcf,'Color',[1 1 1]);
%      string = strcat('Program I: \nu =',int2str(nu./100),'cm^(Eisenlohr et
al.)');
%      title(string);
%      shading interp;

%% _____%%


    phi=angle(psi_complex_reshaped); % gives angles in the range -pi:pi

    if length(nu_array) == 1

        filename =
strcat('psi_peak_program1_vec_n1.9_',num2str(Nx),'x',num2str(Ny),'_',num2st
r(nu_array(1)),'_10micron.mat');

        save(filename,'Xplot','nu');
```

```matlab
g=fopen(['program1_vec_',num2str(nu_array(1)),'_',num2str(NX),'x',num2str(NY),'_',' n1.9_10micron.txt'],'a');
        fprintf(g,'%f      ',nu);
        fprintf(g,'%f\n',IntegralPsi);

        fclose(g);
    else


g=fopen(['program1_vec_',num2str(nu_array(1)),'_',num2str(nu_array(end)),'_',num2str(NX),'x',num2str(NY),'_','_n1.9_10micron.txt'],'a');
        fprintf(g,'%f      ',nu);
        fprintf(g,'%f\n',IntegralPsi);

        fclose(g);

    end
end
```

Appendix C

The MATLAB scripts for program II is enclosed in Appendix C:

- *SpericalWave_Scattering.m*

  The analytical spherical wave scatter method is implemented as an algorithm in this script. Calculates the S matrix and finds the maximum points, and the zero points to the denominator of the S matrix, which gives the same point. An plot the images at this points.

- *constants.m* (function)

  A function that gives the constants *A*, *S* and the denominator of S.

```matlab
%%%%%%%%%%%%%%%%%%%%%%%%%%%%%%%%%%%%%%%%%%%%%%%%%%%%%%%%%%%%%%%%%%%%%%%%%%%%
%     SpericalWave_Scattering.m                                          %
%                                                                        %
%     Frida H.M Torgersen                                                %
%                                                                        %
% Program II based on the analytical spherical wave scattering solution %
%%%%%%%%%%%%%%%%%%%%%%%%%%%%%%%%%%%%%%%%%%%%%%%%%%%%%%%%%%%%%%%%%%%%%%%%%%%%

%% _____ properties that can be changed_____


n = 1.9; % Refractive index
a = power(10,-5); % radius of the disk
M = 0; % order number

nu = (500:1:1400)*100; %wavenumber in cm^-1
lambda = 1./nu;

K = length(nu);

k=2*pi./lambda; % angular wavenumber outside the disk

beta = k*n; % angular wavenumber inside the disk

[A,S,DenominatorS] = constants(M,a,k,beta,n); % Constants from a function

f = real(DenominatorS);

%% _____Plotting S_m_____
y = strcat('S_' ,int2str(M)); % Write S_m(k) for m = 0,1,2 or 3
figure()
plot(nu*0.01,real(S),'lineWidth',1.5)
grid on
legend(y,'Location','Best')
title(y)
```

```matlab
xlabel('nu')
ylabel(y)
%% _____ Plott denominator of S_m_____
y = strcat('denominator of S_' ,int2str(M)); % Write S_m(k) for m = 0,1,2
or 3
figure()
plot(nu*0.01,f,'lineWidth',1.5)
grid on
legend(y,'Location','Best')
title(y)
xlabel('nu')
ylabel(y)
%% _____ find zeros to the denominator of S_m_____

[indx] = cross_points(f); % function cross_points.m  finds the index to the
point before cross point y=0

k_a = k(indx); % gives the x-point before the cross point
k_b = k(indx+1); % gives the x-point after the cross point

for i = 1:length(k_a)
    x_1 = k_a(i);
    x_2 = k_b(i);
    k_zeros(i) = find_zeros(x_1,x_2,n,a,M);
end



%% Plot of the den_S = 0

    % Plot the wave functions
for p = 1:length(k_zeros)
    k = k_zeros(p);
    beta = k*n;
    [A,S,DenominatorS] = constants(M,a,k,beta,n);
    X0=-2*a;
    Y0=-2*a;

    Nstep=200; % Choose a even number for section plot!
    Psi=zeros(Nstep,Nstep);
    step=4*a/Nstep;

    for i=1:Nstep
        x=X0+step*double(i);
        for j=1:Nstep
            y=Y0+step*double(j);
            theta1=atan2(y,x);
            r1=sqrt(x*x+y*y);
            if (r1<a)
                psi=besselj(M,beta*r1)*exp(1i*M*theta1);
                Psi(j,i)= A*psi;
            elseif (r1>a)
                h1=besselh(M,2,k*r1)*exp(1i*M*theta1);
                h2=S*besselh(M,1,k*r1)*exp(1i*M*theta1);
                Psi(j,i)=h1+h2;


            end
        end
    end


X
```

```matlab
    nu = k./(2*pi*100);
    ZAbsWaveFunction.d=abs(Psi).*abs(Psi);



    if(1)
        figure;
        set(gcf,'Color',[1 1 1]);
        pcolor(ZAbsWaveFunction.d);
        shading interp;
%         colorbar;
        k_string = strcat('S_', int2str(M),':','nu_' ,int2str(p), ' = ',
int2str(nu),'cm^(Eisenlohr et al.)');
        title(k_string);
    end


end
```

```matlab
%%%%%%%%%%%%%%%%%%%%%%%%%%%%%%%%%%%%%%%%%%%%%%%%%%%%%%%%%%%%%%%%%%%%%%%%%%%
%     constants.m                                                        %
%                                                                        %
%     Frida H.M Torgersen                                                %
%                                                                        %
%     A function that gives three constants A, S and the DenominatorS.   %
%%%%%%%%%%%%%%%%%%%%%%%%%%%%%%%%%%%%%%%%%%%%%%%%%%%%%%%%%%%%%%%%%%%%%%%%%%%


function [A,S,DenominatorS] = constants(M,a,k,beta,n)

    for j = 1:length(k)
        J = besselj(M,beta(j)*a);
        if M == 0
            dJ = -n*besselj(1,beta(j)*a);     %dJ_0 = -J_1
        else
            dJ = 0.5*n*(besselj(M-1,beta(j)*a)-besselj(M+1,beta(j)*a));
        end

        H1 = besselh(M,1,k(j)*a);
        H2 = besselh(M,2,k(j)*a);
        if M == 0
            dH1 = -besselh(1,1,k(j)*a); % dH1_0 = -H1_1
            dH2 = -besselh(1,2,k(j)*a); % dH2_0 = -H1_2
        else
            dH1 = 0.5*(besselh(M-1,1,k(j)*a)-besselh(M+1,1,k(j)*a));
            dH2 = 0.5*(besselh(M-1,2,k(j)*a)-besselh(M+1,2,k(j)*a));
        end


        NominatorA(j) = H1*dH2-H2*dH1;
        DenominatorA(j) = dJ*H1-J*dH1;

        A(:,j) = NominatorA(j)./DenominatorA(j);

        NominatorS(j) = H2*dJ - J*dH2;
        DenominatorS(j) = J*dH1 -dJ*H1;

        S(:,j) = NominatorS(j)./DenominatorS(j);



    end

end
```